BIOCHEMISTRY

The CDK1-TOPBP1-PLK1 axis regulates the Bloom's syndrome helicase BLM to suppress crossover recombination in somatic cells

Chiara Balbo Pogliano[1]†, Ilaria Ceppi[2]†, Sara Giovannini[1]†, Vasiliki Petroulaki[3], Nathan Palmer[3], Federico Uliana[1], Marco Gatti[4], Kristina Kasaciunaite[5], Raimundo Freire[6,7,8], Ralf Seidel[5], Matthias Altmeyer[4], Petr Cejka[1,2]*, Joao Matos[1,3]*

Bloom's syndrome is caused by inactivation of the BLM helicase, which functions with TOP3A and RMI1-2 (BTR complex) to dissolve recombination intermediates and avoid somatic crossing-over. We show here that crossover avoidance by BTR further requires the activity of cyclin-dependent kinase-1 (CDK1), Polo-like kinase-1 (PLK1), and the DDR mediator protein TOPBP1, which act in the same pathway. Mechanistically, CDK1 phosphorylates BLM and TOPBP1 and promotes the interaction of both proteins with PLK1. This is amplified by the ability of TOPBP1 to facilitate phosphorylation of BLM at sites that stimulate both BLM-PLK1 and BLM-TOPBP1 binding, creating a positive feedback loop that drives rapid BLM phosphorylation at the G_2-M transition. In vitro, BLM phosphorylation by CDK/PLK1/TOPBP1 stimulates the dissolution of topologically linked DNA intermediates by BLM-TOP3A. Thus, we propose that the CDK1-TOPBP1-PLK1 axis enhances BTR-mediated dissolution of recombination intermediates late in the cell cycle to suppress crossover recombination and curtail genomic instability.

INTRODUCTION

Homologous recombination plays an essential role in the maintenance of genome integrity by repairing DNA breaks caused by DNA damaging agents or upon breakdown of stalled replication forks (*1*, *2*). As its hallmark feature, homologous recombination establishes interactions between homologous DNA molecules and can lead to the formation of four-way intermediate structures, also known as Holliday junctions (HJs) (*3*, *4*). Despite being generated to facilitate DNA repair, HJs are potentially toxic intermediates, as a single unprocessed HJ could result in chromosome nondisjunction and aneuploidy (*5*).

Enzymes that process HJs have been identified in all domains of life, from a variety of organisms including bacteriophage, bacteria, archaea, yeast, and humans (*6*, *7*). In mitotically dividing human cells, the primary pathway for HJ processing relies on a four-subunit complex, BLM-TOP3A-RMI1-RMI2 (BTR), also known as the "dissolvasome." The dissolvasome catalyzes the convergent migration of two HJs involving coordinated activities of the BLM helicase and the TOP3A topoisomerase. The last predicted intermediate of branch migration is a hemicatenate that can be dissociated by topoisomerase action (*6*, *8*). BLM is mutated in individuals with Bloom's syndrome (BS). A diagnostic feature of cells derived from patients with BS is an elevated frequency of sister chromatid exchanges (SCEs), in which genetic material is reciprocally exchanged between the two recombining DNA molecules through crossing-over (*9*, *10*). Although SCEs are, in principle, not mutagenic, SCEs are indicators of increased interhomolog crossovers, which can lead to loss of heterozygosity of tumor suppressor genes (*11*). In agreement with this notion, individuals with BS develop a broad spectrum of early-onset cancers driven by genomic instability (*12*, *13*).

The cellular function of BTR in the processing of recombination intermediates is complemented by structure-selective endonucleases. In human cells, three nucleases have been implicated in HJ "resolution," namely, GEN1, MUS81-EME1, and SLX1-SLX4 (*14*–*19*). GEN1 dimerizes on HJs and introduces two symmetrically related incisions across the junction point (*20*). SLX1-SLX4 and MUS81-EME1 act within the same protein complex, termed SMX, to nick and counternick HJs, respectively (*21*, *22*). The lack of a bias in the directionality of HJ cleavage by structure-selective endonucleases gives rise to the formation of crossovers and noncrossovers as products of recombination. As HJ dissolution, mediated by BTR, gives rise exclusively to noncrossovers, dissolution is critical for crossover avoidance. The compensatory activity of structure-selective endonucleases drives the high frequency of SCEs in cells from individuals with BS (*8*, *23*, *24*).

In mitotically dividing cells, the formation of noncrossovers by dissolution is thought to be predominant because GEN1 and SMX are activated toward the end of the cell cycle in response to rising cyclin-dependent kinase 1 (CDK1) activity (*5*, *25*, *26*). GEN1 is excluded from the nucleus during the early stages of the cell cycle (*27*). Only upon nuclear envelope breakdown, which is triggered by CDK1 (*28*), the GEN1 nuclease gains access to chromatin (*27*, *29*). CDK1 activity also promotes the cell cycle stage–specific association of MUS81-EME1 with SLX1-SLX4 to form the SMX holoenzyme at the G_2-M transition (*21*, *30*). Therefore, by processing DNA intermediates not acted upon by the dissolvasome, structure-selective endonucleases are thought to function as safeguards of chromosome segregation and genome stability. In contrast to HJ resolution, HJ dissolution is presumed to occur much earlier in the cell cycle, but experiments to directly address this model have been lacking.

[1]Institute of Biochemistry, ETH Zürich, Otto-Stern-Weg 3, 8093 Zürich, Switzerland. [2]Institute for Research in Biomedicine, Faculty of Biomedical Sciences, Università della Svizzera italiana (USI), 6500 Bellinzona, Switzerland. [3]Department of Chromosome Biology, Max Perutz Labs, University of Vienna, Vienna Biocenter, Vienna, Austria. [4]Department of Molecular Mechanisms of Disease, University of Zurich, Winterthurerstrasse 190, 8057 Zürich, Switzerland. [5]Peter Debye Institute for Soft Matter Physics, Universität Leipzig, 04103 Leipzig, Germany. [6]Unidad de Investigación, Hospital Universitario de Canarias–FIISC, Ofra s/n, 38320 La Laguna, Tenerife, Spain. [7]Instituto de Tecnologías Biomédicas, Universidad de La Laguna, Tenerife, Spain. [8]Universidad Fernando Pessoa Canarias, 35450 Las Palmas de Gran Canaria, Spain.
*Corresponding author. Email: petr.cejka@irb.usi.ch (P.C.); joao.matos@univie.ac.at (J.M.)
†These authors contributed equally to this work.

Whereas HJ resolving enzymes are tightly cell cycle regulated, it is unclear whether analogous mechanisms regulate BTR-mediated HJ dissolution. In budding yeast, the BLM ortholog helicase Sgs1 is phosphorylated by S phase $Cdc28^{CDK}$, which increases its general ability to unwind recombination intermediates in vitro and in vivo (*31*). $Sgs1^{BLM}$ is further phosphorylated by Polo-like kinase (PLK) Cdc5 (PLK1 in humans) at the G_2-M transition, but the function of this second cell cycle–regulated modification is unknown (*31*). $Cdc5^{PLK1}$ is the mitotic kinase responsible for the activation of yeast $Mus81\text{-}Mms4^{EME1}$ and $Yen1^{GEN1}$ resolvases, suggesting a model in which cell cycle–regulated phosphorylation establishes a hierarchy in pathway usage: Sgs1-Top3-Rmi1 (STR) dissolvasome acts first, during S phase, while $Mus81\text{-}Mms4^{EME1}$ and $Yen1^{GEN1}$ are activated at the onset of mitotic division (*27*, *31*, *32*).

Although it is unknown whether BTR-mediated HJ dissolution is cell cycle regulated in human cells, BLM is known to have S phase functions, for example, in DNA end resection at the onset of recombination or in the restart of stalled replication forks (*33*–*36*). On the other hand, BLM has been reported to interact with the mitotic PLK1 (*37*) and to be phosphorylated in a CDK-dependent manner at the G_2-M transition (*38*). Phosphorylation of BLM at serine-304, which lies within a minimal CDK consensus motif, promotes interaction with the DNA damage response (DDR) mediator protein TOPBP1 and plays a role in the suppression of SCE formation in chicken DT40 cells (*39*). Precisely how TOPBP1 functions to suppress crossover recombination is unknown.

In this work, we show that BTR, CDK1, PLK1, and TOPBP1 act within the same genetic pathway to suppress somatic crossovers and genomic instability. We show that CDK1 and TOPBP1 synergize to facilitate robust binding and phosphorylation of BLM by PLK1, which stimulates BLM-TOP3A–mediated dissolution of recombination intermediates in vitro and in vivo. As CDK1 and PLK1 are maximally active at the G_2-M transition, our data suggest that, in human cells, dissolution occurs much later in the cell cycle than anticipated.

RESULTS

CDK1- and PLK1-mediated phosphorylation of BLM in vitro and in vivo

We have previously shown that phosphorylation of *Saccharomyces cerevisiae* $Sgs1^{BLM}$ stimulates its ability to unwind DNA joint molecules during S phase (*31*). To determine whether this regulatory mechanism is conserved in evolution, we asked whether BLM is similarly modified in mitotically dividing human cells. To this end, we synchronized HeLa cells at the G_1-S phase of the cell cycle and followed the electrophoretic mobility of BLM as cells progressed through S phase, upon synchronous release from a double thymidine block. At G_1-S, BLM migrated as a single band, which slightly decreased in intensity as cells passed through S phase (2 to 4 hours after G_1-S release) (Fig. 1, A and B). Besides the slight fluctuation in expression levels, we found no evident S phase–linked phosphorylation-dependent electrophoretic mobility shift of BLM, in contrast to $Sgs1^{BLM}$ as described previously (*40*).

In addition to the Cdc28/CDK-mediated modification in S phase, $Sgs1^{BLM}$ is further phosphorylated by Cdc5/PLK1 at the onset of M phase (*31*). In line with this modification, we observed a marked decrease in the electrophoretic mobility of BLM as cells accumulated M phase markers, including PLK1, cyclin B (CycB), and phosphorylated Cdc27 (a CDK1 target; Fig. 1, A and B) (*41*). The electrophoretic mobility of immunoaffinity-purified BLM^{VFLAG}, ectopically expressed in M phase–arrested cells, sharply increased upon treatment with λ-phosphatase (Fig. 1C). This suggests that BLM is phosphorylated during the late stages of the cell cycle, which is in agreement with previous reports that BLM becomes modified upon nocodazole-mediated arrest of cells at prometaphase (*37*, *38*).

Next, we sought to determine whether CDK1 and PLK1 might be involved in the modification of BLM at G_2-M. To this end, we compared the electrophoretic mobility of BLM in cells treated with CDK1 or PLK1 inhibitors (CDK1i and PLK1i) and nocodazole (Fig. 1D). In agreement with the timing of the phospho-shift, which correlates with the peaks of CycB and PLK1 expression (Fig. 1, A and B), both CDK1 and PLK1 activities were necessary for the full extent of BLM modification at G_2-M (Fig. 1, E and F). A reduction in the BLM mobility shift was also observed when cells were pre-synchronized at prometaphase and acutely treated with CDK1i or PLK1i, in both HeLa (Fig. 1, G to I) and hTERT-RPE1 cells (fig. S1A). By contrast, inhibition of the checkpoint kinase CHK1 or the DDR kinase ATR, which were previously implicated in phosphorylating BLM after DNA damage (*42*) or after replication stress (*43*), had no detectable effect on the G_2-M phase modification of BLM (Fig. 1, F and I, and fig. S1B).

Given the involvement of CDK1 and PLK1 in modifying BLM in vivo, we asked whether these two kinases were able to phosphorylate recombinant BLM in vitro. Both human CDK1-CycB complex and PLK1 were able to phosphorylate recombinant BLM (Fig. 1J and fig. S1, C and D). Combining CDK1-CycB with PLK1 led to an additive increase in the phosphorylation of BLM (Fig. 1, J and K). In light of the observation that acute CDK1 inhibition in cells causes a more pronounced increase in the electrophoretic mobility of BLM, when compared to PLK1 inhibition (Fig. 1I), it is likely that CDK1 functions upstream of PLK1, possibly acting as a priming kinase to regulate PLK1-BLM binding. Together, these data suggest that BLM is phosphorylated by CDK1 and PLK1 at the G_2-M transition in human cells. The phosphorylation timing of BLM differs from yeast $Sgs1^{BLM}$, which is modified sequentially in S phase and M phase (*40*).

PLK1 kinase activity prevents MUS81-mediated SCEs in mitosis

To determine whether the G_2-M phosphorylation of BLM is relevant for its function, we sought to investigate whether CDK and PLK1 are required for the suppression of crossover recombination. In human cells, crossover formation can be assayed by the detection of SCEs on mitotic chromosome spreads (*10*). Because CDK1 activity is required for the G_2-M transition, thus precluding the condensation of chromosomes in cells treated with CDK1i, we initially focused on PLK1. Cells treated with PLK1i 6 hours before mitotic shake-off (Fig. 2A) displayed an increased incidence of SCEs (Fig. 2, B and C). Similar results were obtained with hTERT-RPE1 cells (Fig. 2, D and E) and simian virus 40 (SV40)–transformed fibroblasts (GM00637) (Fig. 2, F and G), indicating that the PLK1i-driven increase in SCE formation is cell line independent. Small interfering RNA (siRNA)–mediated depletion of PLK1 also led to increased levels of SCEs (fig. S2, A and B), confirming the specificity of the results obtained with the PLK1i.

Because SCE formation could occur as a consequence of abnormal levels of DNA damage/replication stress (*44*), we asked whether PLK1 inhibition might lead to activation of the DDR kinases ATM and ATR (*45*). Western blot and quantitative image–based

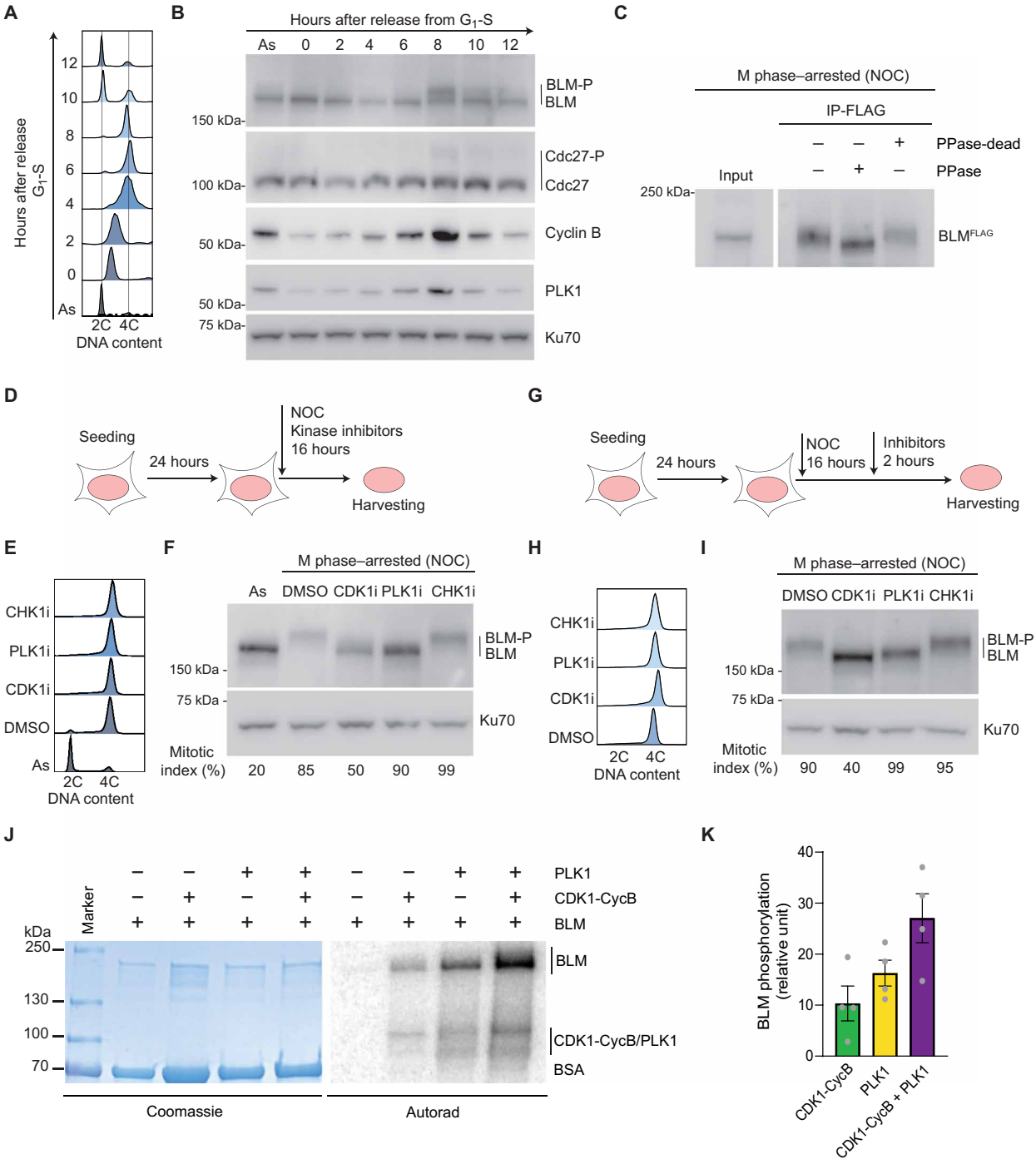

Fig. 1. In vitro and in vivo phosphorylation of BLM by the cell cycle kinases CDK1 and PLK1. (**A**) HeLa Kyoto cells were synchronized at G_1-S with a double thymidine block. Samples were collected at 2-hour intervals after release from thymidine. The DNA content was analyzed by fluorescence-activated cell sorting. As, asynchronously proliferating cells. (**B**) A fraction of the samples collected as in (A) was analyzed by Western blotting for the indicated proteins. (**C**) HeLa cells ectopically expressing BLM^{FLAG} were synchronized in mitosis by nocodazole (NOC) treatment. FLAG immunoprecipitates (IPs) from total cell extracts were then treated with λ-phosphatase (PPase) or heat-inactivated λ-phosphatase (PPase-dead) and analyzed by Western blotting. (**D**) Experimental design: HeLa cultures are simultaneously treated with NOC and kinase inhibitors for 16 hours. (**E**) The DNA content of cells treated as in (D) was analyzed by FACS. DMSO, dimethyl sulfoxide. (**F**) Lysates from cells treated as in (E) were analyzed by Western blotting for the indicated proteins. Mitotic cell rounding was monitored by light microscopy and expressed as mitotic index (%). (**G**) Experimental design: Subconfluent HeLa cultures are treated with NOC and, 16 hours later, with specific kinase inhibitors for an additional 2 hours. (**H**) The DNA content of cells treated as in (G) was analyzed by FACS. (**I**) Lysates from cells in (H) were analyzed by Western blotting for the indicated proteins. Mitotic cell rounding was monitored by light microscopy and expressed as mitotic index (%). (**J**) CDK1-CycB and PLK1 phosphorylate BLM in vitro. Purified BLM was incubated with purified CDK1-CycB (a model CDK), PLK1, or both kinases. Left: Coomassie-stained proteins after polyacrylamide gel electrophoresis. Right: Autoradiograph of the identical gel. (**K**) Quantitation of the radioactive signal compared to background from experiments such as shown in (J). $n = 4$; error bars, mean ± SEM.

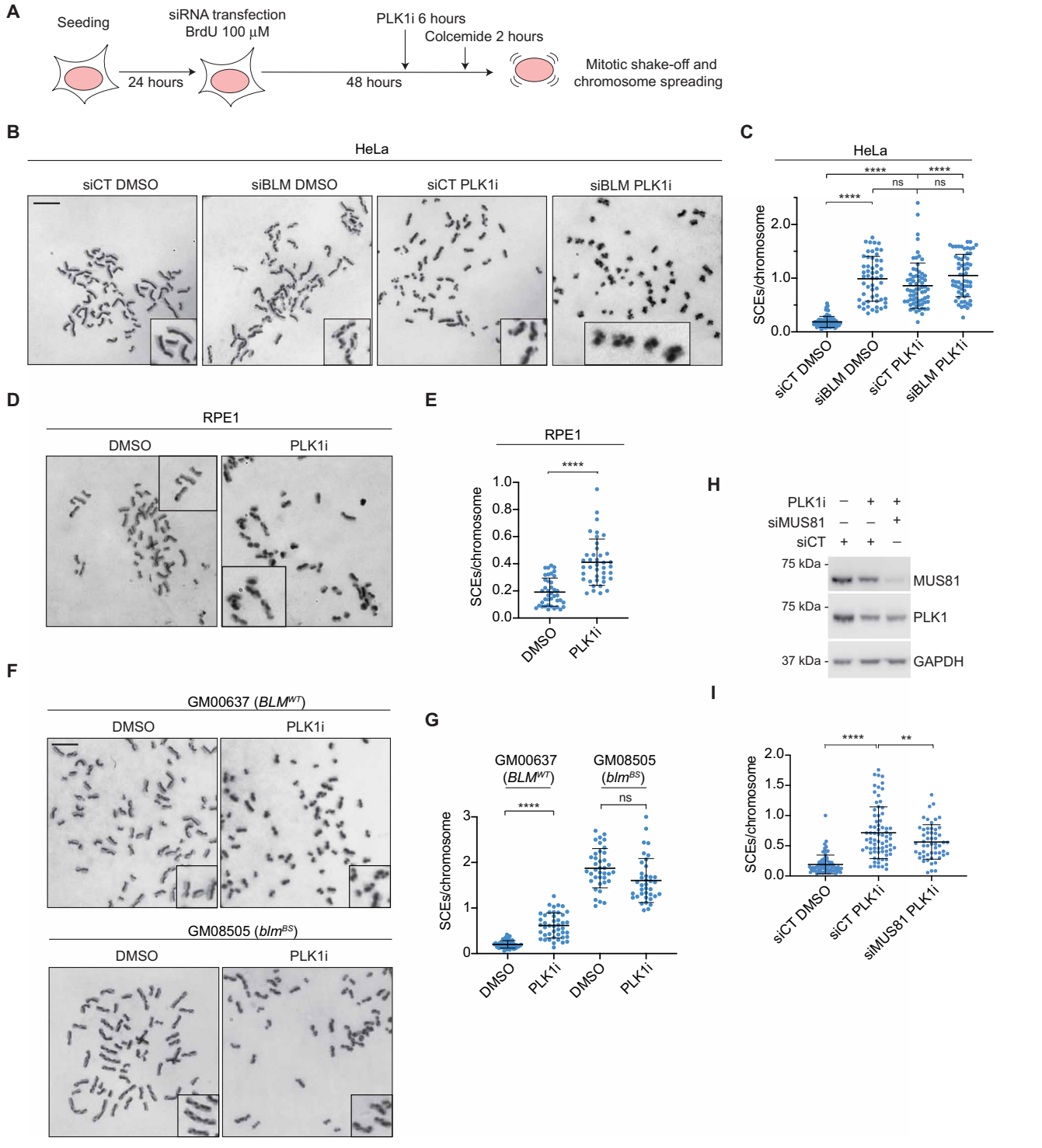

Fig. 2. PLK1 kinase activity prevents SCEs in mitotically dividing cells. (**A**) Schematic representation of the experimental setup to monitor PLK1i (BI2536)–induced SCEs. BrdU, bromodeoxyuridine. (**B**) Representative images of metaphase spreads prepared from HeLa cells treated as described in (A). Control siRNAs (siCT) or siRNAs targeting BLM (siBLM) were used as indicated. (**C**) Quantification of SCE frequency per chromosome, per metaphase spread, of cells in (B). Each data point represents the mean number of SCEs per chromosome in one metaphase. At least 60 metaphases (>5000 chromosomes) were analyzed per condition, in three biological replicates. Black lines represent the mean number of SCEs per chromosome ± SD. Asterisks indicate significant differences [not significant (ns), $P > 0.05$; $^{**}P < 0.01$; and $^{****}P < 0.0001$; two-tailed *t* test. (**D**) As in (B) for hTERT-RPE1 cells. (**E**) As in (C) for hTERT-RPE1 cells. (**F**) Representative images of metaphase spreads prepared from BLM-deficient cells (GM08505; *blm*^{BS}) or control cells (GM00631; *BLM*^{WT}), treated as indicated and described in (A). (**G**) Quantification as in (C) of SCE frequency per chromosome and per metaphase spread of cells such as in (F). (**H**) Western blot analysis of the indicated proteins from lysates of cells treated with the indicated siRNAs and PLK1i (BI2536). GAPDH, glyceraldehyde phosphate dehydrogenase. (**I**) Quantification of SCE frequency as in (C) of cells prepared as in (H). Scale bar, 10 μm.

cytometry (QIBC) analysis of phosphorylated KAP1, RPA, and γ-H2AX showed that HeLa cells treated with PLK1i accumulated with a G_2 DNA content while showing basal levels of DNA damage/replication stress markers (fig. S2, C and D). This observation was in stark contrast to cells treated with WEE1 inhibitors, which displayed elevated KAP1, RPA, and γ-H2AX phosphorylation, as previously described (*30*). These findings suggest that the increase in SCE formation upon PLK1 inhibition is unlikely to be a consequence of PLK1i-induced DNA damage but instead due to loss of BLM function. Thus, we queried whether PLK1 and BLM are components of the same genetic pathway in suppressing SCEs. To do so, we compared the frequency of SCEs in cells treated with PLK1i, siRNAs targeting BLM (siBLM), or both. Notably, siBLM and PLK1i led to a similar increase in SCE formation, which remained comparable when both treatments were combined (Fig. 2, B and C). Similar results were obtained when we treated BLM-deficient cells (GM08505), derived from a patient with BS, with PLK1i (Fig. 2, F and G), revealing that the inhibition of PLK1 is not additive with the stable loss of BLM. We note that the level of SCEs in BS cells was much higher than in control cells (GM00637) treated with PLK1i (Fig. 2, F and G) or in cells transiently depleted of BLM (Fig. 2, B and C). This difference could be caused by incomplete siRNA-mediated depletion of BLM or by the accumulation of genomic rearrangements/mutations over many generations in BS cells, as suggested by the unexpected finding, further discussed below, that BS cells express low levels of the DDR protein TOPBP1 (Fig. 5H).

The data above suggest that PLK1 and BLM are likely components of the same cellular pathway that suppresses mitotic SCEs. SCEs that form when BLM is inactivated are known to arise as a consequence of the actions of structure-selective endonucleases, MUS81 in particular (*21*, *23*). We thus anticipated that the elevated SCEs in cells treated with PLK1i would involve MUS81. In agreement with this prediction, depletion of MUS81 led to a reproducible reduction in SCE formation in cells treated with PLK1i (Fig. 2, H and I, and fig. S2, E and F). We conclude that PLK1 functions with BLM to suppress MUS81-mediated crossing-over.

Until now, it has been assumed that BLM-mediated HJ dissolution is active early in the cell cycle and that, later in the cell cycle, structure-selective endonucleases process recombination intermediates that escaped the attention of the BTR dissolvasome. Our data link BLM-mediated crossover avoidance to the activity of PLK1, suggesting that dissolution may only be completed much later than previously thought.

Two minimal CDK consensus sites in BLM, S144 and S304, are required for the suppression of mitotic crossovers

As mentioned above, the preparation of chromosome spreads is incompatible with the inhibition of CDK1, which precludes mitotic entry. Therefore, to test whether CDK1 is required for the function of BLM, we generated a *BLM* construct encoding for alanine substitutions in all putative CDK sites. BLM contains 13 minimal CDK consensus sites (S/TP), 11 of which have been found to be phosphorylated in vivo (Fig. 3A). We also introduced silent mutations to render BLM^{13A} siRNA resistant and generated a similar construct with wild-type *BLM* (BLM^{WT}). Both BLM^{WT} and BLM^{13A} were then placed under the control of a doxycycline-inducible promoter, C-terminally fused to a Venus-FLAG tag (herein with VFLAG), and integrated as a single copy into the genome of HeLa Flp-IN T-REx cells. Ectopically expressed BLM^{WT} and BLM^{13A} accumulated to comparable levels in both asynchronous and M phase–arrested cells (Fig. 3B). However, whereas the electrophoretic mobility of both proteins was similar in asynchronous cultures (Fig. 3B, left), BLM^{13A} showed a reduced phosphorylation-dependent mobility shift when cells were synchronized in M phase (Fig. 3B, right). This result further strengthens a model in which CDK1 modifies BLM at G_2-M.

Having a phosphorylation-resistant BLM, whose expression was siRNA resistant (fig. S3A), allowed us to interrogate whether BLM^{13A} prevented SCE formation in cells treated with siBLM. Notably, cells expressing BLM^{13A} displayed an elevated level of SCEs, comparable to control cells treated with siBLM. By contrast, the corresponding ectopic BLM^{WT} construct suppressed SCE accumulation in cells treated with siBLM (Fig. 3, C and D). Immunoprecipitation experiments revealed that BLM^{13A} was proficient at interacting with TOP3A (fig. S3B), indicating that the 13 alanine substitutions are unlikely to affect the assembly of the BTR complex.

Next, we sought to dissect the individual contribution of the 13 S/TP residues. Since CDK phosphorylation is known to serve as a priming event for PLK1 binding, we mutated S144, S1290, and S1296, which lie within the Polo-box binding consensus S-S^P/T^P-P motif (*37*, *46*). In addition, we also mutated S304, which does not fully conform to the Polo-box binding consensus but has been shown to mediate BLM binding to TOPBP1 (*39*). The rationale for the inclusion of S304A was based on the finding that TOPBP1 interacts with PLK1 (*47*), which could constitute an alternative mechanism to facilitate BLM phosphorylation. The combined mutation of S144, S304, S1290, and S1296 severely impaired the ability of BLM to suppress SCE formation, without interfering with the stability of BLM or its ability to interact with TOP3A (Fig. 3, E to G). Because the four mutated sites are split between the N terminus (S144 and S304) and the C terminus (S1290 and S1296) of BLM (Fig. 3A), we also generated $BLM^{S144A,S304A}$ cells. $BLM^{S144A,S304A}$ also failed to complement the phenotype resulting from the depletion of endogenous BLM (Fig. 3F), suggesting that S144 and/or S304 may constitute the critical residues. To further test this, we compared SCE formation in cells expressing $BLM^{S144A,S304A}$ with the individual mutations. Cells expressing BLM^{S304A} were indistinguishable from $BLM^{S144A,S304A}$ cells or control cells treated with siBLM, in agreement with S304 being fully required for BLM function (Fig. 3, H and I). On the other hand, cells expressing BLM^{S144A} showed intermediate SCE levels, indicating that S144 is important for BLM function, but not as prominently as S304 (Fig. 3, H and I).

Given the loss-of-function phenotypes observed for BLM^{S304A} and BLM^{S144A}, we determined whether any of the other 13 S/TP sites contribute to SCE suppression by BLM. If S144 or S304 were the only residues whose phosphorylation is necessary for BLM function, then one prediction would be that mutating back A304 to serine, in BLM^{13A}, should lead to a phenotype comparable to the BLM^{S144A} single mutant. In agreement with this prediction, $BLM^{12A,S304WT}$ displayed intermediate SCE levels, comparable to cells expressing BLM^{S144A} (Fig. 3, J and K). When we instead corrected A144 back to S144, to generate $BLM^{12A,S144WT}$, we observed a more severe phenotype, consistent with S304 having a critical role in promoting BLM function (Fig. 3, J and K).

Last, to test whether the phosphorylation of S144 and S304 is required for the BLM-PLK1 interaction, we immunoaffinity-purified BLM from cells synchronized in M phase and probed the immunoprecipitates (IPs) for the presence of PLK1. PLK1 could be detected in BLM^{WT} IPs but was reduced in BLM^{S144A}, BLM^{S304A}, and

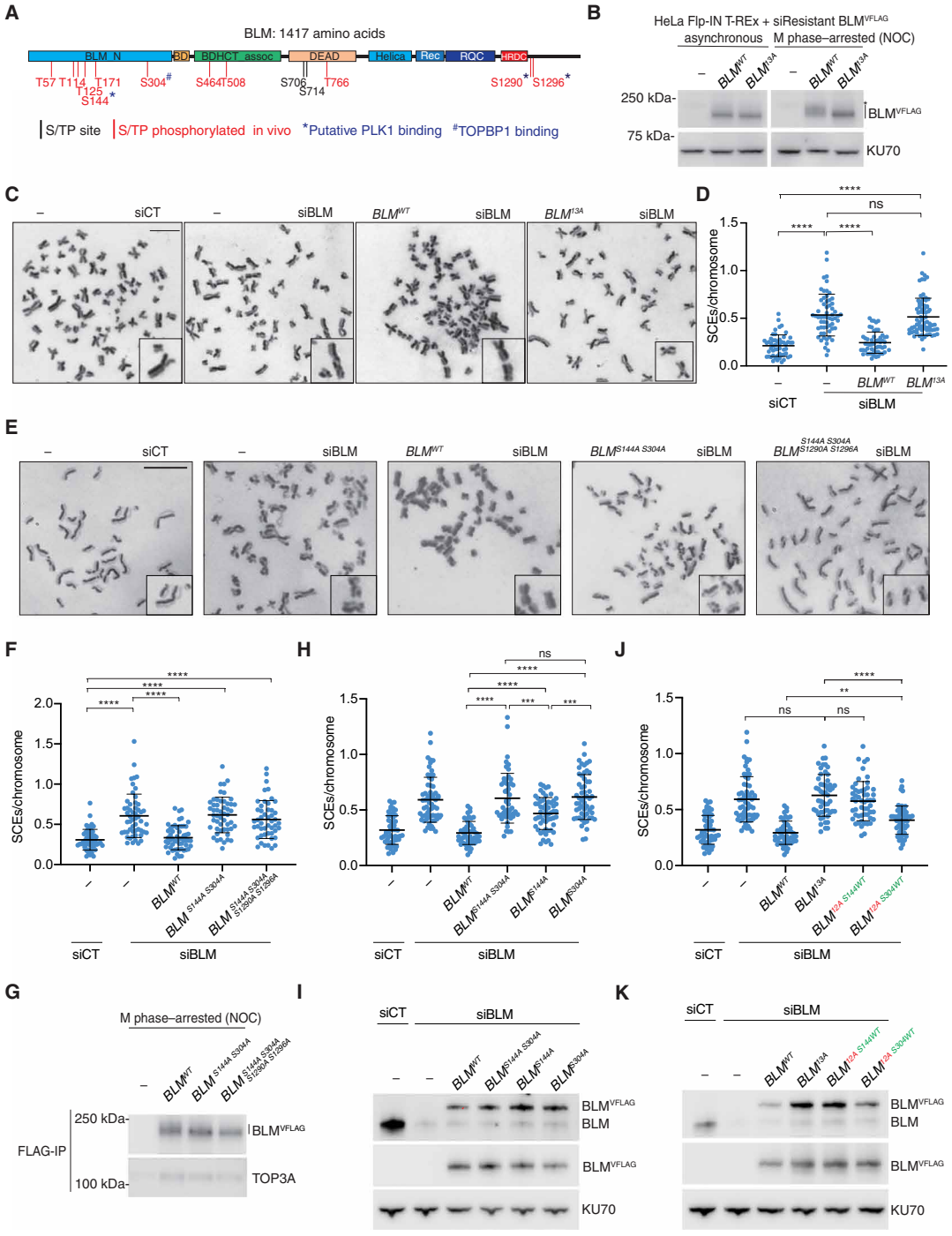

Fig. 3. Phosphorylation of two CDK minimal consensus sites is required for the anti-crossover function of BLM. (**A**) BLM representation with highlighted S/TP sites. Red sites are phosphorylated in vivo (www.phosphosite.org). Blue sites are involved in PLK1 (*) or TOPBP1 (#) binding. (**B**) Western blot analysis of the indicated proteins in lysates from asynchronous or nocodazole-treated HeLa Flp-IN T-REx cells ectopically expressing VFLAG-tagged BLM^{WT} or BLM^{13A}, treated with doxycycline for 48 hours. *Cross-reacting band. (**C**) Representative images of SCEs in spreads from HeLa cells ectopically expressing siRNA-resistant VFLAG-tagged BLM variants. Cells were treated with the indicated siRNAs. (**D**) Quantification of SCE frequency per chromosome, per metaphase spread, of cells as in (C). Each data point represents the mean number of SCEs per chromosome in one metaphase. More than 60 metaphases were analyzed per condition, in three biological replicates. Black lines represent the mean ± SD. Asterisks indicate statistical significance (ns, $P > 0.05$; *$P < 0.05$; **$P < 0.01$; ***$P < 0.001$; and ****$P < 0.0001$; two-tailed t test). (**E**) Representative images of SCEs in cells expressing the indicated BLM variants treated as in (C). (**F**) Quantification of SCE frequency of cells in (E) performed as in (D). (**G**) HeLa cells ectopically expressing the indicated BLM variants were treated with nocodazole. FLAG-IPs were analyzed by Western blotting for the indicated proteins. Parental cells (–) were used for specificity control. (**H**) Quantification of SCEs in cells treated with the indicated siRNAs and ectopically expressing the indicated BLM variants. More than 40 metaphases were analyzed per condition as in (D). (**I**) Western blot analysis of the indicated proteins in cultures as in (H). (**J**) SCE frequency in spreads prepared from cells expressing the indicated BLM variants as in (H). (H) and (J) were performed in parallel and share the siCT and siBLM controls. (**K**) Western blot analysis of the indicated proteins in lysates from samples of cultures as in (J). Scale bar, 10 μm.

$BLM^{S144A,S304A}$ mutants (Fig. 4A and fig. S4A), suggesting that S144 and S304 phosphorylation, and by inference also CDK activity, facilitates the BLM-PLK1 interaction. One possible caveat of using the BLM^{S144A} and BLM^{S304A} mutants to infer a role for CDK1 is that the serine/alanine substitutions could impair the BLM-PLK1 interaction because of the inherent differences between serine and alanine and not because of the lack of alanine phosphorylation. A second limitation is that, although CDK phosphorylates BLM in vitro and in vivo [Figs. 1 (F, I, and J) and 3B] and S144 and S304 are found within minimal CDK consensus sites, it is possible that their phosphorylation is regulated by additional kinases, which could act redundantly with CDK. Hence, to formally test whether CDK activity at G_2-M is required for the BLM-PLK1 interaction, we immunoprecipitated BLM^{FLAP} from M phase–arrested cells acutely treated with CDK1i (30 min). Notably, CDK1 inhibition led to a nearly complete reduction in PLK1 levels in the BLM^{FLAP} IPs, which was accompanied by an increase in the electrophoretic mobility of BLM, consistent with CDK phosphorylation being strictly required for the BLM-PLK1 interaction (Fig. 4B).

To determine whether the BLM-TOPBP1 interaction was similarly sensitive to CDK1 inhibition, we probed the BLM^{FLAP} IPs for the presence of TOPBP1. Although TOPBP1 could be detected in the BLM^{FLAP} IPs, comparable TOPBP1 amounts were also found in IPs from control cells lacking BLM^{FLAP} expression (Fig. 4B), which precluded any conclusion. To circumvent this problem, we immunoprecipitated endogenous TOPBP1 using anti-TOPBP1 antibodies, which were efficiently and specifically enriched for BLM (Fig. 4C). Acute inhibition of CDK1 did not reduce BLM levels in the TOPBP1 IPs, despite triggering an increase in the electrophoretic mobility of both TOPBP1 and BLM and disrupting the TOPBP1-PLK1 association (Fig. 4C). These data suggest that CDK promotes BLM and TOPBP1 phosphorylation, as well as the association of both proteins with PLK1, during G_2-M. The BLM-TOPBP1 interaction, on the other hand, is insensitive to CDK1 inhibition, possibly suggesting that S304 phosphorylation is only required for the initial TOPBP1-BLM association but not for its maintenance. This could be explained if TOPBP1 and BLM associated in the absence of phosphorylation or, alternatively, if S304 phosphorylation was protected from dephosphorylation in states of low CDK1 activity. As mentioned above, yet another possibility is that other kinases could promote BLM S304 modification. Nevertheless, our data demonstrate that the integrity of S144 and S304 in BLM is required for crossover avoidance. As will be presented below, recombinant $BLM^{S144A,S304A}$ per se displays normal levels of helicase activities, suggesting that BLM modification and association with cofactors including CDK1, PLK1, and TOPBP1 are required to promote the activity of the dissolvasome.

TOPBP1 regulates BLM phosphorylation in vitro and in vivo

The data above suggest that two mechanisms may be at play in promoting the BLM-PLK1 interaction and, ultimately, BLM phosphorylation. The first involves S144, a Polo-box binding consensus site (*37*), and the second involves S304, which could mediate a more indirect interaction, via TOPBP1. To test this model, we asked whether BLM can indeed interact with both PLK1 and TOPBP1 directly. To do so, we first obtained purified, and homogeneously phosphorylated, BLM (BLM^P) from *Sf9* cells by including Okadaic acid in the culture medium (fig. S5A), as previously described for Sgs1 (*31*). We then incubated BLM^P with recombinant PLK1 (Abcam) and purified TOPBP1 (also prepared in *Sf9* cells; fig. S1C) and used anti-BLM antibodies to immunoprecipitate BLM complexes. The presence of the interacting proteins in the pull-downs was monitored by Western blotting. Both TOPBP1 and PLK1 efficiently copurified with BLM^P (Fig. 4D, lane 2). Moreover, a direct BLM^P-PLK1 interaction was confirmed when we omitted TOPBP1 (Fig. 4D, lane 3), and conversely, a direct TOPBP1-BLM^P interaction was observed when we omitted PLK1 (fig. S4B, lane 3). Since PLK1 was initially found to be enriched in TOPBP1 IPs from cells (*47*), we also tested whether PLK1 binds TOPBP1 directly, which remained unknown. We found that purified TOPBP1 and PLK1 can interact in vitro (Fig. 4E), establishing that the interaction observed in vivo is most likely direct.

To investigate whether TOPBP1 can simultaneously bind PLK1 and BLM, we turned to mass photometry, a technique that allows us to estimate the molecular weight of protein complexes on the basis of the diffraction of light (*48*). While we could detect the TOPBP1-BLM^P complex (fig. S4C), the TOPBP1-PLK1 and BLM^P-PLK1 complexes were below the limit of detection, indicating a rather transient nature of the interactions, as common for many kinase-protein target interactions. Therefore, we are currently limited in our ability to formally establish whether a complex that simultaneously contains BLM-TOPBP1-PLK1 can stably assemble in cells.

The interaction data above, in combination with the phenotypic analyses of PLK1 inhibition (Fig. 2, B and C) and BLM phospho-resistant mutants (Fig. 3, J and K), hinted that TOPBP1 likely plays a role in regulating the phosphorylation of BLM. To test for this possibility, we transfected cells with siRNAs targeting TOPBP1 and analyzed the electrophoretic mobility of BLM. While PLK1 still accumulated in cells treated with siTOPBP1 and nocodazole, we observed a reduction in the BLM phospho-shift characteristic of M phase (fig. S4D, top). Moreover, the simultaneous depletion of TOPBP1 and PLK1 inhibition did not further noticeably reduce the electrophoretic mobility shift of BLM, suggesting that phosphorylation events on the same sites were affected by the two treatments. As a side but important observation, we did notice that depletion of TOPBP1 also led to a reduction in BLM levels, visible when the depletion of TOPBP1 was nearly complete [fig. S4, D (top) and H to J] (*49*). Therefore, to uncouple the lower expression levels from the impaired electrophoretic mobility shift, we corrected for the imbalance in BLM levels by loading gels with different amounts of total protein but similar levels of BLM. As anticipated, cells treated with siTOPBP1 still showed a reduction in the BLM phospho-shift (fig. S4D, bottom).

The results above indicate that TOPBP1 binds both BLM and PLK1 directly and contributes to BLM phosphorylation at G_2-M. To obtain a more mechanistic insight into the precise function of TOPBP1, we asked whether it altered the ability of CDK and PLK1 to modify BLM in vitro. We reasoned that TOPBP1 could modulate the phosphorylation of BLM by at least two mechanisms: (i) by bringing PLK1 and BLM into close spatial proximity, which could increase the overall efficiency of phosphorylation, and/or (ii) by altering the conformation of BLM, or potentially PLK1, which could enhance the ability of PLK1 to modify a subset of specific residues in BLM. To test for these possibilities, we carried out in vitro BLM phosphorylation reactions by CDK/PLK1 in the presence or absence of purified TOPBP1 (fig. S1C). Because of the large quantities of kinases required for these experiments, we expressed and purified CDK2-CycA (fig. S1C), as it showed similar activity toward BLM when compared side by side with commercial CDK1-CycB (figs. S1D and

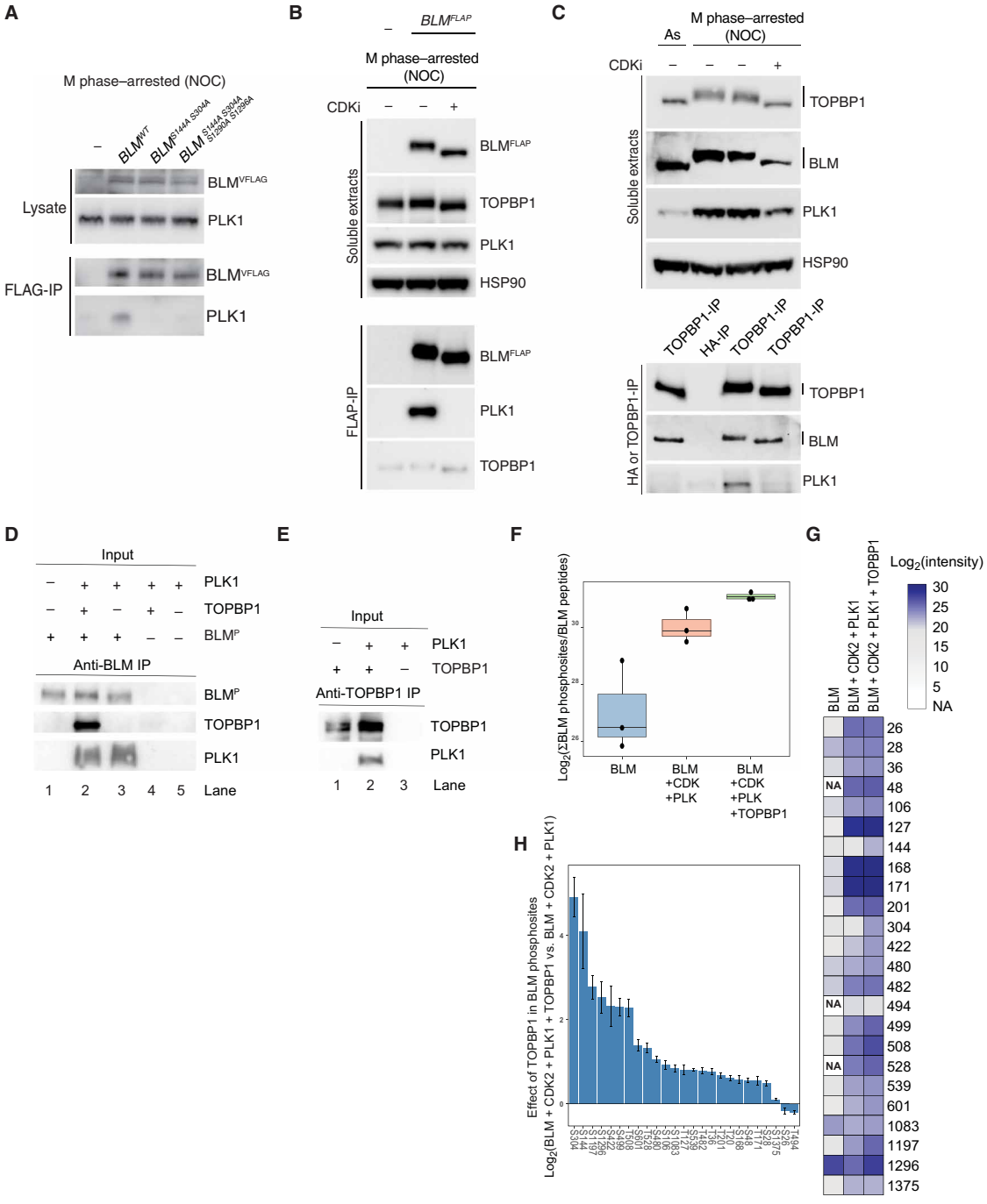

Fig. 4. TOPBP1, CDK, and PLK1 collaborate to promote BLM phosphorylation. (**A**) HeLa cells ectopically expressing the indicated siRNA-resistant BLM^{FLAG} variants were arrested in M phase by nocodazole treatment. FLAG-IPs were analyzed by Western blotting for the indicated proteins. Parental cells (–) were used to control for IP specificity. (**B**) HeLa cells stably expressing BLM^{FLAP} from an integrated BAC were arrested in M phase by nocodazole treatment. CDKi was added 30 min before cell harvesting, as indicated. FLAP IPs [green fluorescent protein (GFP)–IPs] were analyzed by Western blotting for the indicated proteins. Parental cells (–) were used to control for IP specificity. (**C**) Asynchronous HeLa cells (As) were arrested in M phase by nocodazole treatment. CDKi was added 60 min before cell harvesting, as indicated. TOPBP1- or HA-IPs were analyzed by Western blotting for the indicated proteins. (**D**) In vitro analysis of TOPBP1 and PLK1 interaction with BLM^{P}. BLM^{P} was immobilized on Dynabeads Protein G coupled with anti-BLM antibody, and the interaction assay was performed at 100 mM NaCl. The indicated protein was analyzed by Western blotting. (**E**) In vitro analysis of PLK1 interaction with TOPBP1. TOPBP1 was immobilized on Dynabeads Protein G coupled with anti-TOPBP1 antibody, and the interaction assay was performed at 100 mM NaCl. The indicated protein was analyzed by Western blotting. (**F**) Phosphorylation landscape of BLM upon in vitro treatment with CDK2-CycA and PLK1, with or without TOPBP1, as indicated. The sum of all quantified phosphorylation sites normalized for BLM abundance is shown. The experiment was performed in three technical replicates. (**G**) Effect of TOPBP1 on BLM phosphorylation by CDK2-CycA and PLK1. The abundance of the individual phosphorylation sites in each condition was visualized as a heatmap. (**H**) Effect of TOPBP1 on BLM phosphorylation by CDK2-CycA and PLK1. Phosphorylation abundance changes of individual phosphorylation sites are indicated. Means ± SE. NA, not applicable.

S4E); phosphorylated residues were identified and quantified by targeted mass spectrometry (MS) (*50*). When we integrated the intensity of all phosphopeptides detected, normalized by BLM abundance, we observed that the presence of TOPBP1 resulted in a modest increase in the overall ability of CDK/PLK1 to modify BLM (Fig. 4F). However, when we examined in detail the 24 individual phosphorylated residues that could be reproducibly detected, we noticed that the modification of two sites was particularly increased by the presence of TOPBP1: S144 and S304 (Fig. 4, G and H, and fig. S4G). This result suggests that TOPBP1 facilitates the phosphorylation of precisely the two residues that regulate the in vivo interaction with PLK1 (Fig. 4A). We have also noticed that CDK and PLK1 were capable of phosphorylating TOPBP1 in vitro (fig. S4F), consistent with the observation that the G_2-M electrophoretic mobility of TOPBP1 was sensitive to both CDK1i and PLK1i (fig. S1, A and B).

The finding that TOPBP1 stimulates S304 phosphorylation in vitro is intriguing since S304 phosphorylation is itself thought to mediate the TOPBP1-BLM interaction in vivo (*39*). Therefore, one potential explanation for this observation is that S304 phosphorylation may not be strictly required for TOPBP1 binding in vitro or that the alanine substitution disrupts the conserved patch more than nonphosphorylated serine. In agreement with the first possibility, λ-phosphatase–treated BLM^{P} (BLM^{λ}; fig. S5A) retained the ability to interact with TOPBP1 (fig. S4B, lane 4). This result indicates that TOPBP1 may be able to transiently bind unmodified BLM, at least in the absence of competing interactors, and the S304 phosphorylation may be part of a self-reinforcing positive feedback loop that sustains the BLM-TOPBP1, and indirectly the BLM-PLK1, interactions in vivo. This model would be consistent with the observation that the BLM-TOPBP1 interaction in cells is insensitive to CDK1 inhibition (Fig. 4C). Note, however, that we are unable to report at this stage if S304 is efficiently dephosphorylated upon in vitro λ-phosphatase treatment or upon in vivo inhibition of CDK1. It is additionally important to consider that previous structural work with short BLM peptides and the BRCT5 domain of TOPBP1 showed that S304 phosphorylation is important for the BLM-TOPBP1 interaction by promoting electrostatic complementarity between the S304 phosphopeptide and BRCT5 (*51*).

The CDK1-TOPBP1-PLK1 axis suppresses crossover recombination in somatic cells

Our data suggest that phosphorylation of S144 and S304, which is stimulated by TOPBP1 in vitro (Fig. 4H), regulates the function of BLM by promoting PLK1 binding in vivo (Fig. 4A). One prediction of this model is that the combination of BLM^{S144A} or BLM^{S304A} with the inhibition of PLK1 should not lead to an additive increase in the formation of SCEs, as long as the key function of PLK1 in preventing crossovers is to act on BLM. In agreement with this hypothesis, we observed that treatment of cells with PLK1i led to comparable levels in SCE frequency in the presence of BLM^{WT}, BLM^{S144A}, or BLM^{S304A} (Fig. 5, A and B). Moreover, we also found that the depletion of TOPBP1 lead to an increase in SCE frequency similar to that of BLM^{S304A} mutants, which was not further increased when siTOPBP1 was combined with either BLM^{S144A} or BLM^{S304A} (Fig. 5, C and D). Overall, these findings are consistent with TOPBP1 suppressing the formation of SCEs through its ability to bind BLM and regulate its phosphorylation by PLK1.

To ultimately define the relationship between BLM, TOPBP1, and PLK1, we compared the frequency of SCE formation in cells treated with siBLM, siTOPBP1, or PLK1i, as well as the three treatments combined (Fig. 5, E and F). SCE frequency was similarly elevated in all conditions analyzed, pointing toward BLM, TOPBP1, and PLK1 belonging to a single pathway that operates to suppress mitotic crossing-over. This result was further validated by the treatment of BS patient cells lines with siTOPBP1 and PLK1i, which did not significantly change the high frequency of SCEs observed (Fig. 5, G and H). While analyzing the efficiency of siRNA-mediated depletion of TOPBP1, we serendipitously found that the BS patient cell line used expresses extremely low levels of TOPBP1 (Fig. 5H). This finding raises the possibility that long-term loss of BLM may lead to down-regulation of TOPBP1 expression, which could contribute to chronic replication stress/DNA damage and the extremely high SCE levels observed in cells from patients with BS.

In vitro phosphorylation of BLM by PLK1 stimulates the dissolution activity of BLM-TOP3A

To gain mechanistic insights into the regulation of BLM function by phosphorylation, we turned to a reconstituted in vitro system. BLM^{P}, prepared in *Sf*9 insect cells treated with Okadaic acid, exhibited a mobility shift that disappeared after treatment with λ-phosphatase (fig. S5A). Analysis of BLM^{P} by MS revealed modification of at least 58 residues (fig. S5B and data S1). We note that S144 and S304 were not among the residues formally found by MS to be phosphorylated in BLM^{P}. It is however highly likely that their phosphorylation is missed because of concurrent phosphorylation of various additional S/T residues in the respective tryptic peptides (four for S144 and seven for S304). This would be consistent with the observation that we also failed to detect the unphosphorylated peptides containing S144 and S304, which, in the case of S144, could be readily recovered upon λ-phosphatase treatment (fig. S5C).

To our surprise, BLM^{P} (mock-treated) was consistently less active than the corresponding λ-phosphatase–treated polypeptide (BLM^{λ}). Diminished activity of BLM^{P} was observed in assays monitoring the unwinding of plasmid-length double-stranded DNA (dsDNA) (fig. S5D, compare lanes 2 and 3), DNA end resection in conjunction with DNA2 and RPA (fig. S5, D and E), migration and unwinding of an oligonucleotide-based HJ (fig. S5, F to J), and dissolution of a model entangled DNA, which involves the motor activity of BLM and the topoisomerase activity of TOP3A (Fig. 6C and fig. S5, K and L). These results were unexpected, because our previous analysis in vivo suggested a stimulatory function of BLM phosphorylation leading to crossover avoidance (Figs. 1 to 5). Furthermore, *S. cerevisiae* $Sgs1^{P}$ prepared in a similar manner was more active than $Sgs1^{\lambda}$ (*31*), showing that the regulatory control of human BLM and yeast Sgs1 by phosphorylation is likely different. However, it is important to consider that PLK1 impairment was previously reported to result in centromere disintegration upon aberrant BLM-mediated unwinding of centromeric DNA (*52*). Therefore, depending on the cellular context, DNA substrate, respective proteins partners, and the specific residues being modified, BLM phosphorylation may have both positive and negative effects on its biochemical activities.

To define specifically the interplay of BLM with TOPBP1, CDK, and PLK1, we next used dephosphorylated BLM and performed in vitro kinase reactions by CDK/PLK1 in the presence of TOPBP1, which resulted in the phosphorylation of at least 24 residues (Fig. 4G and data S1). Despite being significantly less modified than BLM^{P}, CDK/PLK1-treated BLM was phosphorylated at eight sites that were not detected in BLM^{P} (data S1), indicating that the phosphorylation pattern of BLM in the two

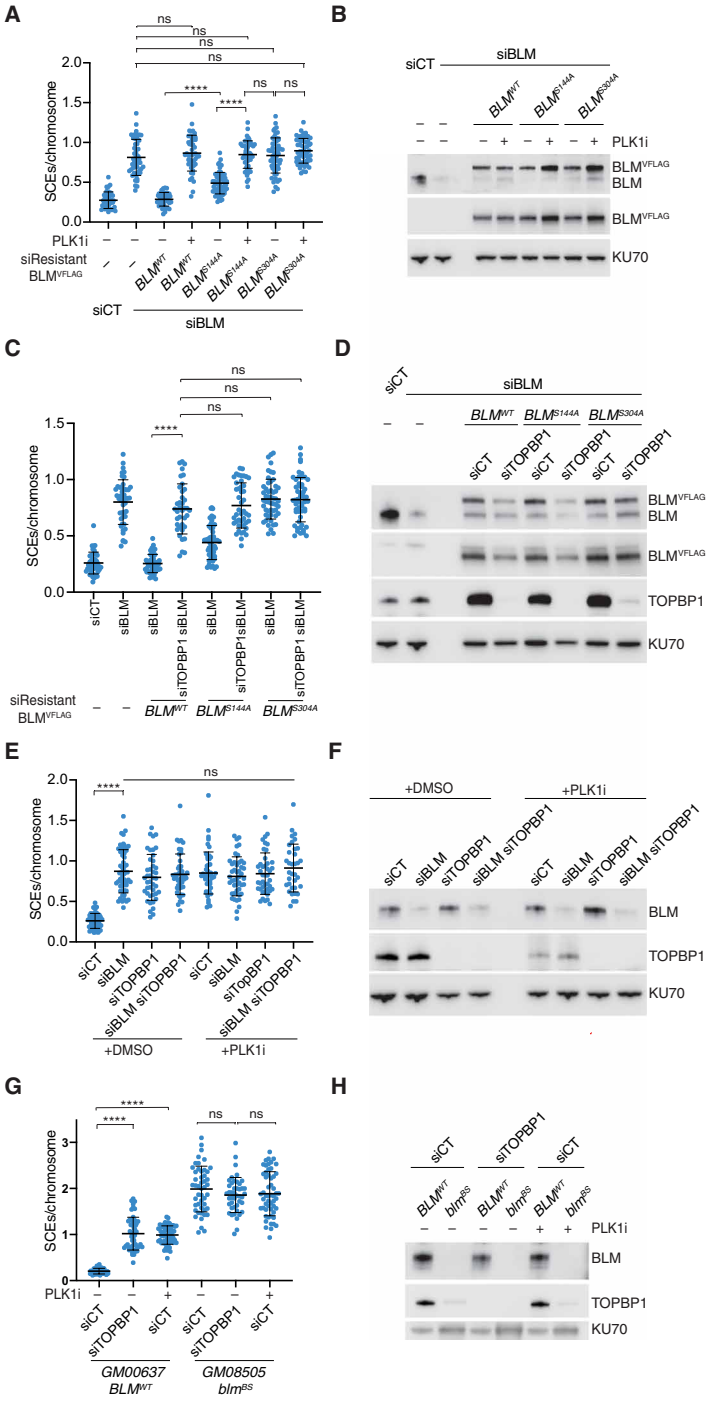

Fig. 5. The CDK1-TOPBP1-PLK1 axis suppresses crossing-over in mitotically dividing human cells. (**A**) Quantification of SCEs in metaphase spreads prepared from HeLa cells ectopically expressing siRNA-resistant FLAG-tagged BLM^{WT}, BLM^{S144A}, or BLM^{S304A}. PLK1i was added to the cultures, or omitted, as indicated, 6 hours before collection and spreading. At least 40 metaphases were analyzed per condition in three biological replicates. Black lines represent the mean number of SCEs per chromosome ± SD. Asterisks indicate significant differences (ns, $P > 0.05$; and ****$P < 0.0001$; one-way ANOVA). (**B**) Western blot analysis of the indicated proteins in lysates from samples of cultures as in (A). (**C**) Quantification of SCEs in metaphase spreads prepared from HeLa cells ectopically expressing siRNA-resistant FLAG-tagged BLM^{WT}, BLM^{S144A}, or BLM^{S304A} as in (A). Cells were additionally transfected with the indicated siRNAs (siBLM or siBLM/siTOPBP1). (**D**) Western blot analysis of the indicated proteins in lysates from samples of cultures in (C). (**E**) Quantification of SCEs in metaphase spreads from HeLa cells transfected with the indicated siRNAs (siCT, siBLM, siTOPBP1, or siBLM/siTOPBP1) as in (A). (**F**) Western blot analysis of the indicated proteins in lysates from samples of cultures in (C). (**G**) Quantification of SCE frequency per chromosome and per metaphase spread of BLM-deficient cells (GM08505; *blm*^{BS}) or control cells (GM00637; *BLM*^{WT}), treated with siCT or siTOPBP1, as indicated. PLK1i was added to cultures, or omitted, as indicated, 6 hours before collection and spreading. Each data point represents the mean number of SCEs per chromosome in one metaphase. At least 60 metaphases were analyzed per condition, in three biological replicates, as in (A). (**H**) Western blot analysis of the indicated proteins in lysates from samples of cultures in (G).

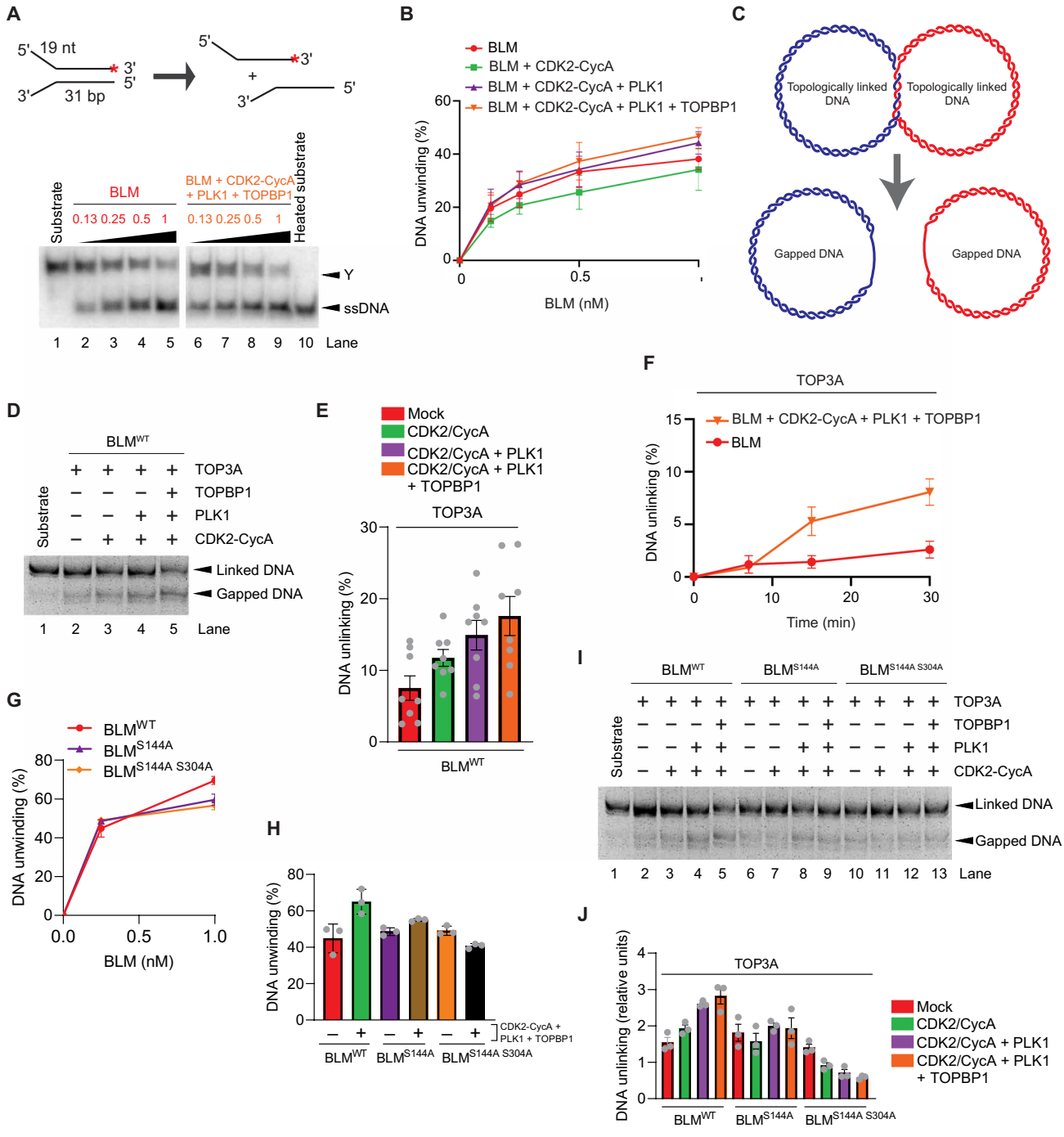

Fig. 6. Phosphorylation of BLM-TOP3A by CDK-PLK1-TOPBP1 increases its dissolution activity. (**A**) Unwinding of Y-structured DNA [19 nucleotides (nt), 31 base pairs (bp)] by in vitro phosphorylated BLM, preincubated with CDK2/CycA, PLK1, and TOPBP1 with 100 mM NaCl and RPA (15 nM). Red asterisks indicate the position of the radioactive label. (**B**) Quantitation of DNA unwinding from experiments such as shown in (A). $n = 3$; error bars ± SEM. (**C**) A schematic representation of the topologically linked DNA substrate used in this study. (**D**) Unlinking of topologically linked DNA by in vitro phosphorylated BLM and TOP3A. Purified BLM was preincubated in an in vitro kinase assay with purified CDK2/CycA, PLK1, and TOPBP1, with 50 mM NaCl and RPA (615.6 nM). (**E**) Quantitation of DNA unlinking from kinetic experiments similar to those as shown in (D). $n = 8$; error bars ± SEM. (**F**) Quantitation of DNA unlinking from kinetic experiments such as shown in (D). $n = 3$; error bars ± SEM. (**G**) Unwinding of Y-structured DNA (25 nt, 25 bp) by BLM variants from experiments such as shown in fig. S6C, as indicated. $n = 3$; error bars ± SEM. (**H**) Unwinding of Y-structured DNA (25 nt, 25 bp) by the indicated in vitro phosphorylated BLM variants (0.25 nM), preincubated with CDK2/CycA, PLK1, and TOPBP1, where indicated. $n = 3$; error bars ± SEM. The values for mock-treated samples were replotted from (G). (**I**) Unlinking of topologically linked DNA by the indicated in vitro phosphorylated BLM variants and TOP3A. Purified BLM variants were preincubated in an in vitro kinase assay with purified CDK2/CycA, PLK1, and TOPBP1, with 50 mM NaCl and RPA (615.6 nM). (**J**) Quantitation of DNA unlinking from experiments similar to those as shown in (I). $n = 3$; error bars ± SEM.

preparations is different. The CDK/PLK1/TOPBP1-treated BLM was not largely affected in its capacity to unwind short Y-structured oligonucleotide-based DNA (Fig. 6, A and B). Notably, however, the CDK/PLK1/TOPBP1-treated BLM was reproducibly more active than mock-treated BLM in the dissolution of a topologically linked DNA substrate, in a reaction requiring the joint functions of BLM and TOP3A (Fig. 6, C to F, and fig. S6A). We noticed that the treatment of BLM with CDK alone already moderately stimulated DNA unlinking, similarly as in reactions with CDK/PLK1 (without TOPBP1). We believe that, in the in vitro reconstitution system, the kinases may have lower substrate specificity. Nevertheless, the greatest stimulation in DNA unlinking was observed when CDK, PLK1, and TOPBP1 were combined with BLM and TOP3A (Fig. 6E).

To verify the importance of the S144 and S304 sites in BLM, we expressed and purified the BLM^{S144A} and $BLM^{S144A,S304A}$ mutants (fig. S6B), which, as expected from the cellular experiments (Fig. 4A), showed reduced binding to PLK1 (fig. S6D). We observed that the BLM variants per se were indistinguishable from the wild-type protein in promoting the unwinding of oligonucleotide-based Y-structured DNA (Fig. 6G and fig. S6C). This result represents an important control also for the cellular experiments, showing that the BLM mutations do not affect its capacity as a helicase, in the absence of cofactors. When BLM was combined with CDK, PLK1, and TOPBP1, we observed a moderate stimulation of DNA unwinding when using Y-structured DNA; this stimulation was not detected when using the BLM^{S144A} and $BLM^{S144A,S304A}$ mutants (Fig. 6H and fig. S6C). The BLM^{S144A} and $BLM^{S144A,S304A}$ variants per se were also as proficient as wild-type BLM in DNA unlinking together with TOP3A, but, notably, the mutants failed to be stimulated by CDK/PLK1/TOPBP1 (Fig. 6, I and J). Moreover, the DNA unlinking activity of the $BLM^{S144A,S304A}$ mutant appeared to be inhibited by CDK/PLK1/TOPBP1, possibly indicating that S144 and S304 play an important role in ensuring that phosphorylation stimulates BLM function, instead of having an inhibitory role, as observed for BLM^{P} prepared in insect cells (fig. S5, J and K).

DISCUSSION

The BS helicase BLM is a critical caretaker of genome integrity with functions in various steps of recombination-mediated DNA double-strand break repair. BLM promotes DNA end resection early in recombination, controls the quality of subsequent strand invasion, and functions within the BTR complex to catalyze the dissolution of double HJs (*6*, *53*). Here, we identified an axis consisting of the mitotic kinases CDK and PLK1, and the adapter protein TOPBP1, that act in the same pathway with BTR to enable HJ dissolution and suppress somatic crossing-over. Furthermore, we delineate the broad mechanism by which CDK, PLK1, and TOPBP1 interplay to regulate BTR function and, in doing so, gather evidence in support of an unexpected model in which HJ dissolution is completed during late stages of the cell cycle, much later than previously thought.

Regulation of BTR function by cell cycle stage–specific phosphorylation

In agreement with previous observations (*37*, *38*), we find that BLM undergoes cell cycle stage–specific phosphorylation at the G_2-M transition. BLM phosphorylation requires the cyclic activities of CDK1 and PLK1 kinases, which peak precisely at the onset of M phase. Although both kinases are required for efficient BLM phosphorylation, their roles are likely very different. Our data suggest that CDK1 contributes to the phosphorylation of multiple residues within BLM and facilitates PLK1-mediated BLM phosphorylation. BLM S144, which is found within a Polo-box binding motif (*37*), promotes direct BLM-PLK1 binding. BLM S304, which is found within a minimal CDK consensus motif but may not be a direct CDK1 target, further discussed below, appears to regulate PLK1 binding more indirectly by enhancing the association of BLM with TOPBP1 (Fig. 7) (*39*). PLK1 had been previously found to be enriched in TOPBP1 IPs from human cells (*47*). We now show that purified TOPBP1 can bind PLK1 directly. Given that TOPBP1 is required for efficient phosphorylation of BLM by PLK1 and that TOPBP1 binds both BLM and PLK1, we therefore propose that PLK1 phosphorylates BLM within a TOPBP1 environment (Fig. 7). Whether a single molecule of TOPBP1 can simultaneously interact with both BLM and PLK1 remains to be investigated, but the answer to this question may be complicated by the intrinsic ability of TOPBP1 to oligomerize and form phase-separated condensates in vitro and in vivo (*54*, *55*). Our work also indicates that TOPBP1 may act as part of a positive feedback loop that promotes rapid modification of

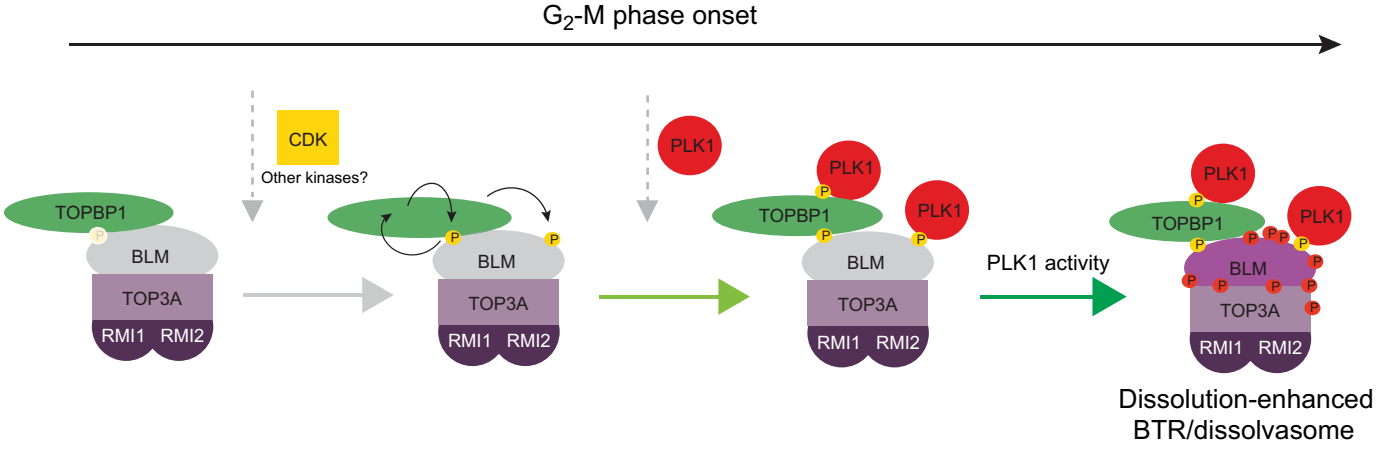

Fig. 7. Working model: Regulated activation of the BTR/dissolvasome complex by the cell cycle kinases CDK1 and PLK1 and the DDR adaptor TOPBP1. CDK1 phosphorylates BLM to promote BLM-PLK1 association and also regulates TOPBP1-PLK1 binding, possibly by phosphorylating TOPBP1. By interacting with BLM and PLK1 and possibly through its ability to form nuclear condensates, TOPBP1 creates a subcellular environment that increases the efficiency of BLM phosphorylation. Ultimately, G_2-M phosphorylation of BLM stimulates the dissolution of topologically linked DNA intermediates by the BTR complex.

BLM at the onset of mitosis. At least in vitro, TOPBP1 stimulates the phosphorylation of S144 and S304, thus possibly enhancing its own ability to interact with BLM and the ability of BLM to directly interact with PLK1 in vivo (Fig. 7). In light of recent work showing that TOPBP1 forms phase-separated nuclear condensates to promote activation of the DDR kinase ATR (*54*), we envisage that TOPBP1 may analogously provide an optimal subcellular environment for efficient modification of BLM by PLK1.

Although CDK promotes the G_2-M phosphorylation of BLM in vivo and phosphorylates BLM in vitro, our data suggest that the BLM-TOPBP1 interaction is insensitive to CDK1 inhibition. Therefore, at present, we cannot distinguish between the following scenarios: (i) CDK1 phosphorylation of BLM S304 occurs in a cell cycle stage–specific manner, but phosphorylated S304 is protected from dephosphorylation during states of low CDK1 activity, possibly by the interaction with TOPBP1. (ii) BLM S304 phosphorylation is sensitive to CDK1 inhibition, but BLM-TOPBP1 complexes remain stable because of S304 phosphorylation–independent interactions. (iii) Other kinase(s) promote S304 phosphorylation to maintain the BLM-TOPBP1 interaction in states of low CDK1 activity. (iv) The previously reported S304A mutation (*39*) could disrupt the BLM-TOP3 interaction because of the intrinsic differences between serine and alanine rather than because of defective phosphorylation. Irrespective of this uncertainty, our data indicate that, in contrast to the BLM-TOPBP1 interaction, the TOPBP1-PLK1 interaction requires high CDK1 activity at G_2-M (Fig. 4C) and TOPBP1 is itself modified in a CDK- and PLK1-dependent manner in vivo (fig. S1B) and in vitro (fig. S4F). Hence, ultimately, the TOPBP1-dependent recruitment of PLK1 is under CDK1 control as well (Fig. 7).

But what is the ultimate function of BLM phosphorylation by PLK1? Our experiments show that in vitro addition of CDK/TOPBP1/PLK1 enhances the ability of BLM to dissolve model entangled DNA in conjunction with TOP3A, without noticeably altering its capacity to unwind simple oligonucleotide-based DNA. Therefore, we propose that PLK1 phosphorylation of BLM enhances the ability of BTR to dissolve late recombination intermediates, explaining the requirement of PLK1 activity in the suppression of MUS81-dependent crossing-over. It is remarkable that hyperphosphorylated BLM purified from insect cells exhibits reduced helicase/translocase-dependent functions. Therefore, it is conceivable that different pools of BLM coexist in cells. In light of this possibility, TOPBP1-mediated phase separation could serve the additional purpose of promoting the formation of different membraneless compartments in which a specific subset of residues is modified, thus locally enhancing or inhibiting a specific function of BLM, a multifaced enzyme. Elucidating these regulatory mechanisms will be an exciting avenue for future research. It will also be interesting to investigate whether the CDK1/PLK1/TOPBP1 cofactors may affect BLM beyond mediating its phosphorylation; specifically, a more direct structural effect of the interactions with the cofactors on BTR activities should be carefully examined.

Cell cycle regulation of HJ-processing enzymes: A revised model

The BLM helicase is thought to function in S and G_2 phases of the cell cycle, which is best demonstrated by its role, together with DNA2, in long-range DNA end resection (*36*). BLM helicase activity in resection can be easily detected by monitoring RPA-coated single-stranded DNA (ssDNA) by fluorescence microscopy, which is compatible with cell cycle staging. By contrast, no such "real-time" readout exists for BLM's dissolution activity. In human cells, the footprint of dissolution can only be detected on mitotic chromosome spreads. This led to the reasonable assumption that dissolution similarly takes place early in the cell cycle, and it is therefore temporally separated from resolution, which occurs predominantly at the onset of mitosis (*25*, *26*). The data presented here link the dissolution activity of the BTR complex to the mitotic kinases CDK1 and PLK1, which promote BLM phosphorylation at G_2-M. This suggests that dissolution is completed later in the cell cycle than previously thought. BLM, in conjunction with TOP3A and RMI1/2, was shown to catalyze the decatenation of underreplicated chromosomal DNA in anaphase cells (*56*). Whether CDK1 and PLK1 are similarly required for BLM's function in processing stalled replication intermediates remains to be clarified.

As discussed above, the present work indicates that HJ dissolution by the BTR complex is cell cycle regulated, which provides one more important piece to the puzzle of how crossover control is implemented in human cells. Moreover, it also unveils important differences on how HJ-processing enzymes are regulated in different organisms. Previously, we observed that Sgs1 is already phosphorylated by $Cdc28^{CDK1}$ in S phase, which results in the enhancement of its helicase activity that is required for efficient processing of recombination intermediates. Sgs1 undergoes additional phosphorylation in M phase by $Cdc5^{PLK1}$, but the functional relevance of this modification remained unclear (*31*). $Cdc5^{PLK1}$ is the mitotic kinase responsible for the activation of yeast $Mus81\text{-}Mms4^{EME1}$ resolvase (and indirectly also $Yen1^{GEN1}$), suggesting a model in which cell cycle–regulated phosphorylation establishes a hierarchy in pathway usage in yeast: STR/dissolvasome acts first during S phase, while $Mus81\text{-}Mms4^{EME1}$ and $Yen1^{GEN1}$ are activated later in the cell cycle to safeguard chromosome segregation (*27*, *31*, *32*). The present work brings two important variations to the budding yeast model. First, it indicates that the Cdc5 ortholog kinase PLK1 is a prominent regulator of dissolution rather than resolution as observed in yeast (*27*, *32*, *57*, *58*). In other words, whereas Cdc5 is crucial for the formation of both mitotic and meiotic crossovers, PLK1 acts as a suppressor of crossing-over in human cells. This is consistent with previous work showing that PLK1 is dispensable for the assembly of the SMX nuclease at G_2-M (*21*) and with the data presented here showing that MUS81 promotes crossover formation upon PLK1 inactivation. A second implication of this work concerns the lack of a clear temporal hierarchy in pathway usage in human cells. How human cells use the dissolvasome as the primary pathway of HJ processing, to avoid potentially deleterious crossing-over, can no longer be fully explained by the model gathered from experiments in yeast. We anticipate that, also in this regard, the adaptor/scaffold proteins TOPBP1 and SLX4, which serve as the platforms for dissolution or resolution, may have evolved additional roles, perhaps in forming specialized subcellular domains that establish pathway usage and dictate recombination outcome.

Last, we note here that although bulk BLM phosphorylation occurs sharply at the G_2-M transition (Fig. 1B), our data do not exclude a gradient model, in which CDK1 and PLK1 activities slowly build up from S phase and gradually enhance BTR function until a marked burst of CDK1 activity drives entry into M phase and bulk BLM phosphorylation. It is also an intriguing possibility that rewiring of the cell cycle machinery, for example, in response to unscheduled

DNA damage or replication stress, could adjust BTR function to specialized cellular needs. To answer these questions, it will be crucial to develop methodologies to follow the BLM "phosphorylation code" in various cellular contexts. The approaches described here to monitor the functional relevance of BLM phosphorylation in vitro and in vivo should be of help in guiding these studies.

MATERIALS AND METHODS

Tissue culture and cell lines

Following procedures previously described in (*30*), HeLa FRT/TO cells, HeLa Kyoto cells, and SV-transformed GM00637 and GM08505 (BS) fibroblasts were maintained in Dulbecco's modified Eagle's medium (DMEM), supplemented with 10% fetal bovine serum (FBS; or Tet-free FBS). U2OS cells were maintained in RPMI 1640 medium, supplemented with 10% FBS. hTERT-RPE1 were maintained in DMEM/F-12, GlutaMAX supplement (catalog no. 31331093) with 10% FBS, 1% penicillin/streptomycin, and hygromycin B (0.01 mg/ml). All cultures were grown at 37°C in a humidified atmosphere containing 5% CO_2.

Stable HeLa FRT/TO cell lines modified with siRNA-resistant versions of VFLAG BLM (BLM^{WT}, BLM^{S144A}, BLM^{S304A}, $BLM^{S144A,S304A}$, $BLM^{S144A,S304A,S1290A,S1296A}$, $BLM^{12A,S144WT}$, $BLM^{12A,S304WT}$, and BLM^{13A}) were induced to express BLM^{VFLAG} with doxycycline (1 mg/ml) 48 hours before harvesting. Stable clones expressing comparable levels of BLM^{VFLAG} and BLM^{VFLAG} derivatives were used in all experiments. BLM^{VFLAG} constructs were made siRNA resistant by the introduction of five silent wobble mutations in the region targeted by the siRNA.

pcDNA5/FRT/TO-Venus-Flag-Gateway (1124) was a gift from J. Pines (Addgene, plasmid no. 40999). BLM^{VFLAG} variants were prepared by gene synthesis of small fragments (GeneArt, Thermo Fisher Scientific), which replaced specific regions in BLM through restriction cloning. BLM was obtained from pcDNA3.1-BLM-FLAG (provided by P. Janscak) (*59*). HeLa Kyoto cells stably expressing BLM^{FLAP} (FLAP is TEV-Speptide-PreScission-EGFP) from a bacterial artificial chromosome under the native regulatory sequences were generated by bacterial artificial chromosome (BAC) recombineering, as previously described (*60*).

siRNA transfections

For siRNA-mediated protein depletion, cells were plated 12 to 24 hours before transfection to a confluency of ~30%. Cells were transfected using Lipofectamine RNAiMAX (Thermo Fisher Scientific). The sequences (5′ to 3′) are as follows: CT (nonspecific control), UAAUGUAUUGGAACGCAUA (*30*); MUS81, CAGCCCUGGUGGAUCGAUA (*23*, *30*); BLM, UCCCGGGAUACUGCUCUCA; PLK1, CGAGCUGCUUAAUGACGAG (*61*); TOPBP1_1, ACAAAUACAUGGCUGGUUATT (*39*); and TOPBP1_2: GCACAAGGUUUAAUGAGGATT (*39*). Protein depletion efficiency was monitored by Western blotting 48 hours after transfection.

Synchronization and mitotic time courses

To obtain cell cycle stage–specific synchronization, following procedures previously described in (*30*), subconfluent cells were treated for 18 hours with thymidine (2 mM) or for 16 to 17 hours with nocodazole (150 ng/ml). To follow the progression of G_1-S arrested cells into mitosis, cells were synchronized with a double thymidine block (15 hours) and released into prewarmed medium containing appropriate amounts of the following kinase inhibitors (or equivalent volumes of the appropriate solvents): 500 nM WEE1 (MK-1775, Selleck Chemicals), 150 to 200 nM PLK1i (BI2536, Selleck Chemicals), 9 μM CDK1i (RO-3306, Sigma-Aldrich), 150 nM CHK1i (AZD-7762), and 3 nM ATRi (AZ-20). The mitotic index was calculated by determining the fraction of rounded-up cells to the total number of cells and expressed as percentage. Images were acquired using a Leica DM IL microscope with an Olympus C-7070 wide zoom camera. More than 200 cells were inspected per condition.

Analysis of SCEs in metaphase spreads

Cells were seeded and incubated in the dark with 100 μM bromodeoxyuridine for 48 hours. Cells were then treated with colcemid (0.2 μg/ml) 2 hours before collection by mitotic shake-off (6 hours for hTERT-RPE1 cells), washed in phosphate-buffered saline (PBS), and swollen in 75 mM KCl for 15 min at 37°C. Ice-cold methanol/acetic acid (3:1 ml) was added, and the cells were centrifuged for 5 min at 180 relative centrifugal force at room temperature. The two-layered solution was removed, and the cells were fixed in 5 ml of ice-cold methanol/acetic acid (15 min on ice). Metaphase cells were then spread on Superfrost microscope slides (Thermo Scientific). After washing with water and air-drying, slides were stained for 20 min with Hoechst 33342 (10 μg/ml) in Sorensen's buffer, as previously described (*62*). After washing with 1× SSC buffer, slides were exposed to long-wavelength (365 nm) ultraviolet light for 30 min. Slides were then immersed in 1× SSC buffer and incubated for 1 hour at 50°C. Samples were immersed in 7% Giemsa in Sorensen's buffer for 15 min at room temperature. After washing with water and air-drying, coverslips were mounted and imaged using an Olympus IX71 microscope outfitted with a DeltaVision Measure system controlled by Softworx software (Applied Precision).

Fluorescence-activated cell sorting analysis of DNA content

Following procedures previously described in (*30*), HeLa cells were treated with trypsin, washed with PBS, and fixed in ice-cold 70% ethanol overnight at 4°C. Before cytometric analysis, cells were washed with PBS and incubated with 50 μl of ribonuclease A (100 mg/ml; QIAGEN) and 200 μl of propidium iodide (50 μg/ml; Sigma-Aldrich). Cellular DNA content was determined using a FACSCalibur flow cytometer (BD Biosciences), and fluorescence-activated cell sorting data were analyzed using FlowJo software.

Protein extraction, immunoprecipitation, and Western blotting

Cells were washed in PBS and lysed in 500 μl of R buffer, as previously described (*63*). Cleared lysates were normalized for total protein content and, when used for immunoprecipitation, incubated with ANTI-FLAG M2 Affinity Gel (A2220, Sigma-Aldrich) or GFP-Trap beads (gta-20, ChromoTek) for 90 min at 4°C (rotating wheel), followed by extensive washing with R buffer. Whole-cell lysates or IPs were subjected to NuPAGE gel electrophoresis (NuPAGE 3 to 8% tris-acetate, NuPAGE 7% tris-acetate, or NuPAGE BOLT 4 to 12% bis-tris; Invitrogen) and blotted onto polyvinylidene difluoride membranes (GE Healthcare). Proteins were detected using mouse anti-MUS81 (Santa Cruz Biotechnology, MTA30 2G10), mouse anti–green fluorescent protein (GFP; Roche), mouse anti-PLK1 (Santa Cruz Biotechnology, sc-17783), rabbit anti-PLK1 (a gift from U. Kutay, ETHZ), mouse anti–γ-H2AX (1:5000; Abcam), rabbit anti–γ-H2AX (Abcam), rabbit anti-KAP1 pS824 (Abcam, ab70369),

mouse anti-CycB (BD), mouse anti-CDC27 (BD), mouse-anti CHK1 (Santa Cruz Biotechnology, sc-8408), rabbit-anti CHK1-S345-P (Cell Signaling Technology), rabbit-anti RPA32 (A300-244 A, Bethyl Laboratories), rabbit-anti RPA32-S33-P (A300-246A, Bethyl Laboratories), rabbit anti-BLM (ab476, Abcam), rabbit anti-BLM (ab2179, Abcam), mouse anti–FLAG-HRP (A8592-1MG, Sigma-Aldrich), rabbit anti-FLAG (F7425, Sigma-Aldrich), rabbit anti-TOPBP1 (ab2402, Abcam), rabbit anti-TOPBP1 (D8G4L, Cell Signaling Technology), and rabbit anti-KU70 (ab92450, Abcam).

High-content microscopy for QIBC

Automated multichannel wide-field microscopy for QIBC of asynchronous HeLa cell populations was performed on the Olympus ScanR High-Content Screening System as described previously (*64*) using a UPLSAPO 20× (0.75 numerical aperture) air objective. Images were analyzed with the in-built Olympus ScanR Image Analysis Software Version 3.0.1; a dynamic background correction was applied, and nuclei segmentation was performed using an integrated intensity-based object detection module based on the DAPI (4′,6-diamidino-2-phenylindole) signal. Downstream analyses were focused on properly detected HeLa cell nuclei containing a 2C to 4C DNA content as measured by total and mean DAPI intensities. Between 1500 and 2500 cells were analyzed for each condition, and single-cell data of cell cohorts of comparable size are shown as color-coded scatterplots generated with Spotfire data visualization software (TIBCO).

Expression and purification of recombinant proteins

Unphosphorylated BLM (BLM) was expressed from pFB-MBP-BLM-His (*65*) in *Sf*9 insect cells using Bac-to-Bac expression system (Invitrogen) and purified by affinity chromatography using amylose (New England Biolabs) and nickel–nitrilotriacetic acid (NTA) agarose (QIAGEN) resins as described (*65*), with the following exception. When bound to the amylose resin, the protein was incubated with λ-phosphatase (New England Biolabs) for 30 min at room temperature in dephosphorylation buffer [50 mM tris-HCl (pH 7.5), 5 mM β-mercaptoethanol, 1 mM phenylmethylsulfonyl fluoride (PMSF), 10% (v/v) glycerol, 300 mM NaCl, and 1 mM $MnCl_2$]. λ-Phosphatase was then washed out, and protein was eluted from the amylose resin. BLM^{P} was purified similarly except that *Sf*9 cells were treated with 50 nM Okadaic acid (APExBIO) for 3 hours before collection and phosphatase inhibitors (50 nM Okadaic acid, 1 mM sodium orthovanadate, 20 mM sodium fluoride, and 15 mM sodium pyrophosphate) were included in the lysis buffer during purification. BLM^{P} was dephosphorylated with λ-phosphatase, resulting in BLM^{λ}. As a "mock" control, λ-phosphatase was not included in the reaction, but the sample was otherwise treated in the same way as the reaction containing λ-phosphatase. BLM^{S144A} and $BLM^{S144A,S304A}$ were obtained by mutating BLM^{WT} plasmid using the QuikChange Mutagenesis Kit according to the manufacturer's recommendation (see Table S1 for the complete primer set). Unphosphorylated or phosphorylated forms of the two mutants were purified as described above for the wild-type protein. Recombinant human CDK1-CycB (catalog no. 14-450) and recombinant human PLK1 (catalog no. ab51426) proteins were purchased from Merck Millipore and Abcam, respectively. $CDK2\text{-}CycA^{\Delta N170}$ complex was expressed in *Escherichia coli* BL21 DE3 pLysS Rosetta cells using the pGEX-GPI-CDK2-Cak1 and the pet21-CycA-ΔN170 plasmids (provided by Pfander laboratory), respectively (*66*). The complex was then purified using Glutathione HiCap Matrix (QIAGEN) and nickel-NTA agarose resin (QIAGEN), as previously described (*66*). TOP3A was expressed in *E. coli* BL21 DE3 pLysS cells using the pET29H2-hTopoIIIα plasmid (provided by Hickson laboratory) according to a previously published procedure (*67*). Frozen pellet from 2 liters of culture was resuspended in lysis buffer [20 mM Hepes-NaOH (pH 7.5), 5 mM β-mercaptoethanol, 0.2 mM EDTA, 1:400 protease inhibitor cocktail (Sigma-Aldrich), leupeptin (30 μg/ml; Merck Millipore), 1 mM PMSF, 30 mM imidazole (Sigma-Aldrich), 0.5 M NaCl, 10% (v/v) glycerol, and 0.1% (v/v) NP-40 (Sigma-Aldrich)]. Lysozyme (0.2 mg/ml) was added to the lysate, and the mixture was incubated at 4°C for 20 min. The sample was sonicated with a probe sonicator (Branson SLPe) at 70% intensity for six rounds of 30 s each. The mixture was centrifuged at 55,000*g* at 4°C for 30 min. The soluble extract was incubated with nickel-NTA agarose resin (QIAGEN) at 4°C for 60 min. The nickel-NTA resin was washed with Ni-NTA wash buffer [20 mM Hepes-NaOH (pH 7.5), 1 mM PMSF, 10% (v/v) glycerol, 1 M NaCl, 30 mM imidazole, and 0.1% (v/v) NP-40]. The last wash was performed with the same buffer but with 180 mM NaCl and no NP-40. Protein was eluted using the Ni-NTA wash buffer without NP-40 and with 150 mM imidazole. Peak fractions, as estimated by the Bradford method, were pooled and diluted by adding four volumes of dilution buffer [20 mM Hepes-NaOH (pH 7.5), 1 mM PMSF, 180 mM NaCl, and 10% (v/v) glycerol]. The diluted fractions were loaded on a HiTrap Heparin HP chromatography column (1 ml/min; GE Healthcare) and washed with buffer A [20 mM Hepes-NaOH (pH 7.5), 0.2 mM EDTA, 10% (v/v) glycerol, 200 mM NaCl, 5 mM β-mercaptoethanol, and 0.1% (v/v) NP-40]. Proteins were eluted using an 8-ml gradient of 200 mM to 1 M NaCl in 0.5-ml fractions in the same buffer. Peak fractions were pooled, snap-frozen in liquid nitrogen, and stored at −80°C. The human TOPBP1 gene was amplified by polymerase chain reaction (PCR) from the pSB147-hTOPBP1 plasmid (a gift from Pfander laboratory) using the TOPBP1_NheI_F and TOPBP1_XmaI_R primers to introduce Nhe I and Xma I restriction sites (see Table S1 for the complete primer set). The PCR product was digested with Nhe I and Xma I restriction endonucleases (New England Biolabs) and ligated into pFB-2xMBP-CtIP-10xHis plasmid (*68*), digested with the same restriction enzymes, to create pFB-2xMBP-TOPBP1-10xHis. The TOPBP1 protein was expressed in *Sf*9 insect cells using the Bac-to-Bac expression system according to the manufacturer's recommendation. Purification was carried out by affinity chromatography using the same buffers and procedure as used for BLM. Human RPA was expressed in *E. coli* (*69*). Briefly, the protein was purified using ÄKTA pure (GE Healthcare) with HiTrap Blue HP, HiTrap desalting, and HiTrap Q chromatography columns (all GE Healthcare). Human DNA2 was expressed in *Sf*9 insect cells and purified by affinity chromatography using the N-terminal 6xHis-tag and the C-terminal FLAG-tag (*65*).

In vitro kinase assays

In vitro phosphorylation reactions were performed in 20-μl volume in kinase buffer [50 mM tris-HCl (pH 7.5), 5 mM magnesium acetate, 0.2 mM EDTA, 100 mM NaCl, 0.5 mM sodium orthovanadate, and 10 mM *p*-nitrophenyl phosphate]. A total of 0.3 μg of BLM, 40 ng of either CDK1-CycB or CDK2-CycA, 40 ng of PLK1, and 0.6 μg of TOPBP1 were added to the reaction, as indicated. All the components were mixed on ice. Reactions were initiated by the addition of 0.1 mM adenosine triphosphate (ATP) and 37 kilobecquerel of

5′-[γ-^{32}P]-ATP (PerkinElmer) and incubated at 37°C for 30 min. Phosphorylated samples were then used for biochemical assays as described below or prepared for autoradiography. In the latter case, phosphorylation reactions were stopped by adding 5 μl of SDS buffer [50 mM tris-HCl (pH 6.8), 1.6% (m/w) SDS, 10% (v/v) glycerol, 0.1 M dithiothreitol (DTT), and 0.01% (w/v) bromophenol blue] and incubated at 95°C for 5 min. Samples were resolved by SDS–polyacrylamide gel electrophoresis, stained with Coomassie dye, and destained in 40% (v/v) methanol and 10% (v/v) acetic acid. The gel was dried on 3MM paper (Whatman), exposed to storage phosphor screen (GE Healthcare), and scanned using Typhoon Phosphor Imager FLA 9500 (GE Healthcare). BLM phosphorylation was performed with CDK1-CycB or CDK2-CycA, which modified BLM with similar efficiency.

Protein interaction assays

To test for interactions between BLM and TOPBP1, 1 μg of purified BLM^{P} was mock- or λ-phosphatase–treated as described above. A total of 10 μl of Dynabeads Protein G (Invitrogen) was conjugated with 0.5 μg of anti-BLM antibody (Abcam, ab476) in PBS-T for 1 hour at 4°C. Next, beads were incubated with pretreated BLM in IP buffer [25 mM tris-HCl (pH 7.5), 1 mM DTT, 3 mM EDTA, bovine serum albumin (BSA; 0.2 mg/ml), and 75 mM NaCl] for 1 hour at 4°C. Beads were then washed three times with wash buffer [50 mM tris-HCl (pH 7.5), 120 mM NaCl, 0.05% (v/v) Triton X-100, 1 mM DTT, and 3 mM EDTA] and incubated for 1 hour at 4°C with recombinant TOPBP1 (1 μg) in IP buffer. Beads were again washed three times with wash buffer, and proteins were eluted by boiling for 3 min in SDS buffer [50 mM tris-HCl (pH 6.8), 1.6% (m/w) SDS, 10% (v/v) glycerol, 0.1 M DTT, and 0.01% (m/w) bromophenol blue]. As a negative control, purified TOPBP1 was incubated with the anti-BLM–coupled Dynabeads that had not been bound by BLM. The proteins in the eluate were analyzed by Western blotting using anti-BLM primary antibody (diluted 1:1000 in 5% milk in TBS-T; Abcam, ab476) or anti-TOPBP1 primary antibody (diluted 1:1000 in 5% milk in TBS-T; Abcam, ab2402) using standard procedures. To detect interaction with PLK1, pull-down experiments were performed as indicated above by conjugating either anti-BLM or anti-TOPBP1 antibodies with Dynabeads Protein G. Beads were then incubated for 1 hour at 4°C with BLM^{P} or TOPBP1 and washed three times with wash buffer. Recombinant PLK1 (1 μg) was then added to the beads in IP buffer, and samples were incubated for 1 hour at 4°C. PLK1 in the eluate was analyzed by Western blotting using anti-PLK1 primary antibody (diluted 1:2000 in 5% milk in TBS-T; Santa Cruz Biotechnology, sc-17783). When the interaction between BLM^{S144A} or BLM^{S144A,S304A} mutants and PLK1 was analyzed, pull-down experiments were performed as indicated above with the exception that a homemade anti-BLM antibody (Freire laboratory) was conjugated with 10 μl of Dynabeads Protein G (Invitrogen).

MS analysis of BLM phosphorylated peptides (data-dependent acquisition and parallel reaction monitoring analysis)

Phosphopeptides generated from the proteolysis of BLM protein (mock or in vitro phosphorylated as described above) were subjected to MS identification and quantification. Briefly, ~2 μg of purified BLM protein was loaded on a centrifugal unit (Vivacon 500, 10MKCO, Sartorius) and centrifuged until dry (centrifugation 8000*g*, 15 min). After denaturation (8 M urea), reduction [5 mM tris(2-carboxyethyl) phosphine (TCEP)], and alkylation (10 mM iodoacetamide), BLM was washed with 25 mM ammonium bicarbonate (three centrifugation steps, 8000*g*, 15 min) and overnight proteolyzed [0.2 μg of trypsin (Promega) sequencing grade]. Proteolysis was quenched by 0.1% trifluoroacetic acid, and dried peptides were resuspended in 10 μl of 0.1% formic acid and 2% acetonitrile supplemented with iRT peptides (Biognosys) for quality control. Identification of targeted peptides was performed by liquid chromatography–tandem MS (LC-MS/MS) operating in data-dependent acquisition (DDA) mode. In a second step, a parallel reaction monitoring (PRM) library [precursor mass/charge ratio (*m*/*z*), fragment *m*/*z*, and retention time] was generated from peptides identified in DDA mode. The library was supplemented with two phosphopeptides (BLM S304 and BLM S144) annotated in the Peptide Atlas database (www.peptideatlas.org/) (*70*). For these peptides, fragments and transitions ions were extracted from the following spectra: https://db.systemsbiology.net/sbeams/cgi/PeptideAtlas/ShowObservedSpectrum?atlas_build_id=502&spectrum_identification_id=4189658078&peptide=VPC[160]IEFDDDDDYDTDFVPPS[167]PEEIISASSSSSK&assumed_charge=3&chimera_level=&sample_id=7463&spectrum_name=H20120618_PM_SPARC1Large_IMAC_05.30589.30589.3 and https://db.systemsbiology.net/sbeams/cgi/PeptideAtlas/ShowObservedSpectrum?atlas_build_id=502&spectrum_identification_id=3962383409&peptide=KLEFSSS[167]PDSLSTINDWDDMDDFDTSETSK&assumed_charge=3&chimera_level=&sample_id=6401&spectrum_name=OR8_121126_EDG_PG_phosJurkat_30min_B3.29190.29190.3. Quantification of targeted peptides was performed by LC-MS/MS operating in PRM mode using library coordinates for the extraction of targeted peptides.

DDA analysis

LC-MS/MS was performed on an Orbitrap Q Exactive+ mass spectrometer (Thermo Fisher Scientific) coupled to an EASY-nLC-1000 liquid chromatography system (Thermo Fisher Scientific). Peptides were separated using a reverse phase column (75 μm ID × 400-mm new objective, in-house packed with ReproSil Gold 120 C18, 1.9 μm, Dr. Maisch GmbH) across 60-min linear gradient from 5 to 35% [buffer A, 0.1% (v/v) formic acid; buffer B, 0.1% (v/v) formic acid and 98% (v/v) acetonitrile]. The DDA mode was set to perform a maximum of 20 scans for the top 20 most intense peptides (TOP20) with MS1 identification (R = 140,000 at 400 *m*/*z*, AGC = 3×10^6, and maximum IT = 110 ms), HCD fragmentation (NCE = 25%), isolation windows (1.4 *m*/*z*), and MS2 identification (R = 35,000 at 400 *m*/*z*, AGC = 1×10^5, and maximum IT = 110 ms). Charge states lower than two and higher than seven were rejected. Acquired spectra were searched using the MaxQuant software version 1.5.2.8 embedded with the Andromeda search engine (*71*) against BLM and TOPBP1 sequences extended with contaminant. The search parameters were set to include only fully tryptic peptides, carbamidomethylation as static peptide modification, and oxidation (M) and phosphorylation (S, T, and Y) as variable modification. The MS and MS/MS mass tolerance were set to 10 and 20 parts per million, respectively. False discovery rate of <1% was used at peptide level. For the identification of BLM phosphosites in the presence or absence of λ-phosphatase, only phosphosites with a localization probability >0.8 were considered. Raw data of DDA files and MaxQuant output files are available via ProteomeXchange with the identifier PXD026452.

For the quantification of BLM phosphosites in the presence of TOPBP1, the spectra library (precursor ion, fragment ions, and

retention time) was generated from phosphopeptides with a localization score >0.95 and with a unique phosphosite. The top three peptides with the highest spectrum score, which are not containing phosphosites and without missed cleavages, were considered for the normalization of protein abundance and added to the library. Raw data of DDA files, MaxQuant output files, and the script for the library generation are available via ProteomeXchange with the identifier PXD026460.

PRM analysis

Targeted analysis was performed using the same chromatography conditions described above for DDA analysis. MS acquisition of the targeted peptide was set up with the combination of one MS1 untargeted scan (R = 70,000 at 400 m/z, AGC = 3×10^6, maximum IT = 100 ms) and 63 scheduled targeted scan (R = 35,000 at 400 m/z, AGC = 5×10^4, maximum IT = 110 ms) using an isolation window of 2.0 m/z and HCD fragmentation (NCE = 27%). Manual curated analysis of fragments was performed using Skyline daily (64 bit, 20.1.1.213 version). Peptide identification was confirmed by the co-elution of at least six fragments at the elution time, in which the peptide was identified in the DDA run (±5 min). As the elution information for two phosphopeptides (S144 and S304) was missing in the spectra library, the identification was based on the co-elution of precursor and transitions ions. The output tables of fragment intensity and Skyline session are provided on PRIDE under the identifier PXD026460. Data analysis of PRM data was performed from the top five most intense fragments; to avoid the integration of noisy transitions, only transitions with an intensity at least 10 times greater compared to the background signal were considered and summed. Last, BLM phosphopeptide intensity was $\log_2$-transformed and normalized on the basis of the intensity of the top two BLM non-phosphorylated peptides.

DNA substrate preparation

Topologically linked DNA substrate was prepared with modified versions of the pUC18 plasmid, in which five and seven recognition sites for ssDNA cutting restriction enzymes (Bbvc I) were inserted to generate 46– and 68–nucleotide (nt)–long single-stranded gaps, respectively (*72*). pG46 and pG68 plasmids were digested using Nt.BbvcI (New England Biolabs) and Nb.BbvcI (New England Biolabs), respectively, at 37°C for 2 hours. The digests were incubated at 85°C for 20 min and then moved on ice immediately. The digests were purified with a QIAquick PCR purification kit (QIAGEN). The structure of each gapped circle was verified by restriction digestion with Spe I restriction endonuclease (New England Biolabs). The gapped circles were mixed in equimolar amounts and were then annealed in 50 mM tris-HCl (pH 7.5) and 10 mM magnesium chloride at 65°C for 15 min and left overnight to reach room temperature. They were subsequently interlinked using *E. coli* topoisomerase I (New England Biolabs) for 30 min at 37°C. The topologically linked DNA structure, comprising the annealed, linked circles, was heated to 80°C for 3 min and then immediately moved on ice to separate those circles that were annealed but not interlinked. The substrate was then gel-purified as described above and was verified by being resistant to heating.

Oligonucleotide-based DNA substrates were radiolabeled at the 3′ terminus with [α-^{32}P]dCTP (deoxycytidine triphosphate; Perkin-Elmer) and terminal transferase (New England Biolabs) according to the manufacturer's instructions (*73*). Unincorporated nucleotides were removed using Micro Bio-Spin P-30 chromatography columns (Bio-Rad). The Y-structured DNA substrate [19 nt, 31 base pairs (bp)] was prepared by labeling of the oligonucleotide X12-3 and annealing with X12-4NC (*65*). The Y-structured DNA substrate (25 nt, 25 bp) was instead prepared by labeling of the oligonucleotide PC1253 and annealing with PC1254 (*74*). For the mobile HJ substrate, the oligonucleotide XO2 was radiolabeled at the 3′ terminus and annealed with XO1. In parallel, a cold annealing reaction was prepared with oligonucleotides XO1c.MM2 and XO2c.MM. Both annealed mixtures were combined and annealed to obtain the final substrate. As dsDNA control, the labeled oligonucleotide XO2 was annealed with the fully complementary oligonucleotide XO2c.MM (*75*). The 2.2-kbp-long randomly labeled dsDNA was prepared as described before (*76*) by amplifying human *NBS1* gene with PCR in the presence of radioactive [α-^{32}P]dCTP.

DNA unlinking assays

DNA unlinking reactions (volume, 10 μl) were carried out in a reaction buffer containing 50 mM tris-HCl (pH 7.5), 5 mM magnesium chloride, 1 mM DTT, BSA (0.1 mg/ml), and 50 mM NaCl. Reactions were assembled on ice with 2.5 nM in vitro phosphorylated BLM, 20 nM TOP3A, and 615.6 nM RPA, as indicated, and preheated at 37°C for 1 min. Unlinking reactions were started by adding 2 mM ATP and 100 ng of topologically linked DNA substrate and incubated at 37°C either for 15 min or for the indicated time points. Reactions were stopped with 5 μl of 2% STOP solution [150 mM EDTA, 2% (m/w) SDS, 30% (v/v) glycerol, and 0.1% (m/w) bromophenol blue] and 1 μl of proteinase K (20.3 mg/ml; Roche) for 10 min at 37°C. DNA was resolved on 1% agarose gel prestained with GelRed (Biotium).

Helicase assays

DNA unwinding assays (volume, 15 μl) were carried out in a reaction buffer containing 25 mM tris-acetate (pH 7.5), 5 mM magnesium acetate, 1 mM DTT, BSA (0.1 mg/ml), 1 mM phosphoenolpyruvate, pyruvate kinase (80 U/ml), 1 mM ATP, 100 mM NaCl, and 0.1 nM ^{32}P-labeled oligonucleotide-based DNA substrate (in molecules). The reactions were assembled on ice, initiated by the addition of ATP, and incubated at 37°C for 30 min. Next, 5 μl of 2% STOP solution [150 mM EDTA, 2% (m/w) SDS, 30% (v/v) glycerol, and 0.1% (w/v) bromophenol blue] and 1 μl of proteinase K (20.3 mg/ml; Roche) was added to stop the reaction for 10 min at 37°C. The 2% STOP solution was supplemented with 20-fold molar excess of the X12-3 cold oligonucleotide to avoid the reannealing of the unwound products. The products were separated on 10% native polyacrylamide gel. The gels were transferred on 17 Chr chromatography paper (Whatman), dried, exposed to storage phosphor screens (GE Healthcare), and scanned using the Typhoon Phosphor Imager FLA 9500 (GE Healthcare).

HJ migration/unwinding assays

HJ migration assays were carried out in 15-μl volume containing 20 mM tris-HCl (pH 7.5), 5 mM magnesium acetate, 1 mM DTT, BSA (0.1 mg/ml), 10% (v/v) glycerol, 100 mM NaCl, 2 mM ATP, and 0.5 nM ^{32}P-labeled oligonucleotide-based DNA substrate (in molecules). RPA was added to the reaction mixture as indicated. The reactions were assembled on ice, initiated by the addition of ATP, and incubated at 37°C for 30 min. Next, 5 μl of 2% STOP solution [150 mM EDTA, 2% (m/w) SDS, 30% (v/v) glycerol, and 0.1% (m/w) bromophenol blue] and 1 μl of proteinase K (20.3 mg/ml;

Roche) were added to stop the reactions for 10 min at 37°C. The products were separated on 8% native polyacrylamide gel, and the gels were transferred on 17 Chr chromatography paper (Whatman) and analyzed as defined for the helicase assays.

Resection assays

Resection assays with PCR-based DNA substrate were performed in 15-µl volume in 25 mM tris-acetate (pH 7.5), 2 mM magnesium acetate, 1 mM ATP, 1 mM DTT, BSA (0.1 mg/ml), 1 mM phosphoenolpyruvate, pyruvate kinase (80 U/ml), 100 mM NaCl, and 1 nM substrate (in molecules). Human RPA was included as indicated to saturate all ssDNAs. After the addition of the other recombinant proteins on ice, the reactions were incubated for 30 min at 37°C. Reactions were stopped by adding 5 µl of 2% STOP solution [150 mM EDTA, 2% (m/w) SDS, 30% (v/v) glycerol, and 0.1% (m/w) bromophenol blue] and 1 µl of proteinase K (20.3 mg/ml; Roche) and incubated at 37°C for 10 min. Samples were analyzed by 1% agarose gel electrophoresis. Gels were dried on DE81 chromatography paper (Whatman), exposed to storage phosphor screens (GE Healthcare), and scanned using the Typhoon Phosphor Imager FLA 9500 (GE Healthcare).

Mass photometry

Mass photometry measurements were executed on a OneMP device (Refeyn Ltd.). Glass coverslips (no. 1.5 H thickness, 24 mm by 50 mm; VWR) were cleaned by 15 min of sonication in isopropanol and deionized water. Afterward, coverslips were dried under a clean stream of nitrogen. For each measurement, the cleaned coverslip was placed onto the objective. For sample delivery, a silicone gasket (CultureWell Reusable Gasket, Grace Bio-Labs) with four wells was fixed on the surface of the coverslip.

Before each measurement, all samples were incubated in measurement buffer [25 mM tris-HCl (pH 7.5), 100 mM NaCl, 3 mM EDTA, and 1 mM DTT] at 4°C for 1 hour. For data acquisition, the gasket well was filled with 9 µl of measuring buffer (room temperature) to allow surface focusing. After that, 1 µl of protein sample was added to the gasket, resulting in a final sample concentration of 5 to 15 nM (5/10 nM BLM^P and 5/10 nM TOPBP1). Protein binding to the coverslip surface was monitored for 100 s using AcquireMP (version 2.3.0; Refeyn Ltd.). Data analysis was performed by DiscoverMP (version 2.3.0; Refeyn Ltd.) and OriginPro 2017. For contrast to mass conversion, a known mass standard calibrant (NativeMark Unstained Protein Standard, Invitrogen) was measured the same day. All samples were measured at least three times.

Statistical analyses

The number of cells or chromosomes analyzed and the number of independent experiments performed are indicated in the figure legends. Error bars on all graphs are SEM or SD. Prism 8 software (GraphPad) was used for statistical analyses.

SUPPLEMENTARY MATERIALS

Supplementary material for this article is available at https://science.org/doi/10.1126/sciadv.abk0221

View/request a protocol for this paper from *Bio-protocol*.

REFERENCES AND NOTES

1. L. Ranjha, S. M. Howard, P. Cejka, Main steps in DNA double-strand break repair: An introduction to homologous recombination and related processes. *Chromosoma* **127**, 187–214 (2018).
2. M. Jasin, R. Rothstein, Repair of strand breaks by homologous recombination. *Cold Spring Harb. Perspect. Biol.* **5**, a012740 (2013).
3. R. Holliday, A mechanism for gene conversion in fungi. *Genet. Res. Camb.* **5**, 282–304 (1964).
4. M. Bzymek, N. H. Thayer, S. D. Oh, N. Kleckner, N. Hunter, Double Holliday junctions are intermediates of DNA break repair. *Nature* **464**, 937–941 (2010).
5. J. Matos, S. C. West, Holliday junction resolution: Regulation in space and time. *DNA Repair (Amst)* **19**, 176–181 (2014).
6. A. H. Bizard, I. D. Hickson, The dissolution of double Holliday junctions. *Cold Spring Harb. Perspect. Biol.* **6**, a016477 (2014).
7. H. D. Wyatt, S. C. West, Holliday junction resolvases. *Cold Spring Harb. Perspect. Biol.* **6**, a023192 (2014).
8. L. Wu, I. D. Hickson, The Bloom's syndrome helicase suppresses crossing over during homologous recombination. *Nature* **426**, 870–874 (2003).
9. N. A. Ellis, D. J. Lennon, M. Proytcheva, B. Alhadeff, E. E. Henderson, J. German, Somatic intragenic recombination within the mutated locus BLM can correct the high sister-chromatid exchange phenotype of Bloom syndrome cells. *Am. J. Hum. Genet.* **57**, 1019–1027 (1995).
10. R. S. Chaganti, S. Schonberg, J. German, A manyfold increase in sister chromatid exchanges in Bloom's syndrome lymphocytes. *Proc. Natl. Acad. Sci. U.S.A.* **71**, 4508–4512 (1974).
11. J. R. LaRocque, J. M. Stark, J. Oh, E. Bojilova, K. Yusa, K. Horie, J. Takeda, M. Jasin, Interhomolog recombination and loss of heterozygosity in wild-type and Bloom syndrome helicase (BLM)-deficient mammalian cells. *Proc. Natl. Acad. Sci. U.S.A.* **108**, 11971–11976 (2011).
12. G. Luo, I. M. Santoro, L. D. McDaniel, I. Nishijima, M. Mills, H. Youssoufian, H. Vogel, R. A. Schultz, A. Bradley, Cancer predisposition caused by elevated mitotic recombination in Bloom mice. *Nat. Genet.* **26**, 424–429 (2000).
13. A. J. van Brabant, R. Stan, N. A. Ellis, DNA helicases, genomic instability, and human genetic disease. *Annu. Rev. Genomics Hum. Genet.* **1**, 409–459 (2000).
14. S. L. Andersen, D. T. Bergstralh, K. P. Kohl, J. R. LaRocque, C. B. Moore, J. Sekelsky, Drosophila MUS312 and the vertebrate ortholog BTBD12 interact with DNA structure-specific endonucleases in DNA repair and recombination. *Mol. Cell* **35**, 128–135 (2009).
15. S. Fekairi, S. Scaglione, C. Chahwan, E. R. Taylor, A. Tissier, S. Coulon, M. Q. Dong, C. Ruse, J. R. Yates III, P. Russell, R. P. Fuchs, C. H. McGowan, P. H. L. Gaillard, Human SLX4 is a Holliday junction resolvase subunit that binds multiple DNA repair/recombination endonucleases. *Cell* **138**, 78–89 (2009).
16. I. M. Muñoz, K. Hain, A.-C. Déclais, M. Gardiner, G. W. Toh, L. Sanchez-Pulido, J. M. Heuckmann, R. Toth, T. Macartney, B. Eppink, R. Kanaar, C. P. Ponting, D. M. J. Lilley, J. Rouse, Coordination of structure-specific nucleases by human SLX4/BTBD12 is required for DNA repair. *Mol. Cell* **35**, 116–127 (2009).
17. J. M. Svendsen, A. Smogorzewska, M. E. Sowa, B. C. O'Connell, S. P. Gygi, S. J. Elledge, J. W. Harper, Mammalian BTBD12/SLX4 assembles a Holliday junction resolvase and is required for DNA repair. *Cell* **138**, 63–77 (2009).
18. S. C. Y. Ip, U. Rass, M. G. Blanco, H. R. Flynn, J. M. Skehel, S. C. West, Identification of Holliday junction resolvases from humans and yeast. *Nature* **456**, 357–361 (2008).
19. X. B. Chen, R. Melchionna, C. M. Denis, P. H. L. Gaillard, A. Blasina, I. van de Weyer, M. N. Boddy, P. Russell, J. Vialard, C. H. McGowan, Human Mus81-associated endonuclease cleaves Holliday junctions in vitro. *Mol. Cell* **8**, 1117–1127 (2001).
20. U. Rass, S. A. Compton, J. Matos, M. R. Singleton, S. C. Y. Ip, M. G. Blanco, J. D. Griffith, S. C. West, Mechanism of Holliday junction resolution by the human GEN1 protein. *Genes Dev.* **24**, 1559–1569 (2010).
21. H. D. Wyatt, S. Sarbajna, J. Matos, S. C. West, Coordinated actions of SLX1-SLX4 and MUS81-EME1 for Holliday junction resolution in human cells. *Mol. Cell* **52**, 234–247 (2013).
22. H. D. Wyatt, R. C. Laister, S. R. Martin, C. H. Arrowsmith, S. C. West, The SMX DNA repair Tri-nuclease. *Mol. Cell* **65**, 848–860.e11 (2017).
23. T. Wechsler, S. Newman, S. C. West, Aberrant chromosome morphology in human cells defective for Holliday junction resolution. *Nature* **471**, 642–646 (2011).
24. Y. Dayani, G. Simchen, M. Lichten, Meiotic recombination intermediates are resolved with minimal crossover formation during return-to-growth, an analogue of the mitotic cell cycle. *PLOS Genet.* **7**, e1002083 (2011).
25. S. C. West, M. G. Blanco, Y. W. Chan, J. Matos, S. Sarbajna, H. D. M. Wyatt, Resolution of recombination intermediates: Mechanisms and regulation. *Cold Spring Harb. Symp. Quant. Biol.* **80**, 103–109 (2015).
26. P.-M. Dehe, P.-H. L. Gaillard, Control of structure-specific endonucleases to maintain genome stability. *Nat. Rev. Mol. Cell Biol.* **18**, 315–330 (2017).
27. J. Matos, M. G. Blanco, S. Maslen, J. M. Skehel, S. C. West, Regulatory control of the resolution of DNA recombination intermediates during meiosis and mitosis. *Cell* **147**, 158–172 (2011).
28. S. Guttinger, E. Laurell, U. Kutay, Orchestrating nuclear envelope disassembly and reassembly during mitosis. *Nat. Rev. Mol. Cell Biol.* **10**, 178–191 (2009).

29. Y. W. Chan, S. C. West, Spatial control of the GEN1 Holliday junction resolvase ensures genome stability. *Nat. Commun.* **5**, 4844 (2014).
30. H. Duda, M. Arter, J. Gloggnitzer, F. Teloni, P. Wild, M. G. Blanco, M. Altmeyer, J. Matos, A mechanism for controlled breakage of under-replicated chromosomes during mitosis. *Dev. Cell* **39**, 740–755 (2016).
31. R. Grigaitis, L. Ranjha, P. Wild, K. Kasaciunaite, I. Ceppi, V. Kissling, A. Henggeler, A. Susperregui, M. Peter, R. Seidel, P. Cejka, J. Matos, Phosphorylation of the RecQ helicase Sgs1/BLM controls its DNA unwinding activity during meiosis and mitosis. *Dev. Cell* **53**, 706–723.e5 (2020).
32. B. Szakal, D. Branzei, Premature Cdk1/Cdc5/Mus81 pathway activation induces aberrant replication and deleterious crossover. *EMBO J.* **32**, 1155–1167 (2013).
33. S. L. Davies, P. S. North, I. D. Hickson, Role for BLM in replication-fork restart and suppression of origin firing after replicative stress. *Nat. Struct. Mol. Biol.* **14**, 677–679 (2007).
34. A.-M. K. Shorrocks, S. E. Jones, K. Tsukada, C. A. Morrow, Z. Belblidia, J. Shen, I. Vendrell, R. Fischer, B. M. Kessler, A. N. Blackford, The Bloom syndrome complex senses RPA-coated single-stranded DNA to restart stalled replication forks. *Nat. Commun.* **12**, 585 (2021).
35. A. V. Nimonkar, J. Genschel, E. Kinoshita, P. Polaczek, J. L. Campbell, C. Wyman, P. Modrich, S. C. Kowalczykowski, BLM-DNA2-RPA-MRN and EXO1-BLM-RPA-MRN constitute two DNA end resection machineries for human DNA break repair. *Genes Dev.* **25**, 350–362 (2011).
36. S. Gravel, J. R. Chapman, C. Magill, S. P. Jackson, DNA helicases Sgs1 and BLM promote DNA double-strand break resection. *Genes Dev.* **22**, 2767–2772 (2008).
37. M. Leng, D. W. Chan, H. Luo, C. Zhu, J. Qin, Y. Wang, MPS1-dependent mitotic BLM phosphorylation is important for chromosome stability. *Proc. Natl. Acad. Sci. U.S.A.* **103**, 11485–11490 (2006).
38. E. Bayart, S. Dutertre, C. Jaulin, R. B. Guo, X. G. Xi, M. Amor-Guéret, The Bloom syndrome helicase is a substrate of the mitotic Cdc2 kinase. *Cell Cycle* **5**, 1681–1686 (2006).
39. A. N. Blackford, J. Nieminuszczy, R. A. Schwab, Y. Galanty, S. P. Jackson, W. Niedzwiedz, TopBP1 interacts with BLM to maintain genome stability but is dispensable for preventing BLM degradation. *Mol. Cell* **57**, 1133–1141 (2015).
40. R. Grigaitis, A. Susperregui, P. Wild, J. Matos, Characterization of DNA helicases and nucleases from meiotic extracts of S. cerevisiae. *Methods Cell Biol.* **144**, 371–388 (2018).
41. J. M. Peters, R. W. King, C. Hoog, M. W. Kirschner, Identification of BIME as a subunit of the anaphase-promoting complex. *Science* **274**, 1199–1201 (1996).
42. S. Kaur, P. Modi, V. Srivastava, R. Mudgal, S. Tikoo, P. Arora, D. Mohanty, S. Sengupta, Chk1-dependent constitutive phosphorylation of BLM helicase at serine 646 decreases after DNA damage. *Mol. Cancer Res.* **8**, 1234–1247 (2010).
43. A. Franchitto, P. Pichierri, Bloom's syndrome protein is required for correct relocalization of RAD50/MRE11/NBS1 complex after replication fork arrest. *J. Cell Biol.* **157**, 19–30 (2002).
44. I. Waisertreiger, K. Popovich, M. Block, K. R. Anderson, J. H. Barlow, Visualizing locus-specific sister chromatid exchange reveals differential patterns of replication stress-induced fragile site breakage. *Oncogene* **39**, 1260–1272 (2020).
45. A. N. Blackford, S. P. Jackson, ATM, ATR, and DNA-PK: The trinity at the heart of the DNA damage response. *Mol. Cell* **66**, 801–817 (2017).
46. A. E. H. Elia, P. Rellos, L. F. Haire, J. W. Chao, F. J. Ivins, K. Hoepker, D. Mohammad, L. C. Cantley, S. J. Smerdon, M. B. Yaffe, The molecular basis for phosphodependent substrate targeting and regulation of Plks by the Polo-box domain. *Cell* **115**, 83–95 (2003).
47. P. Moudry, K. Watanabe, K. M. Wolanin, J. Bartkova, I. E. Wassing, S. Watanabe, R. Strauss, R. Troelsgaard Pedersen, V. H. Oestergaard, M. Lisby, M. Andújar-Sánchez, A. Maya-Mendoza, F. Esashi, J. Lukas, J. Bartek, TOPBP1 regulates RAD51 phosphorylation and chromatin loading and determines PARP inhibitor sensitivity. *J. Cell Biol.* **212**, 281–288 (2016).
48. A. Sonn-Segev, K. Belacic, T. Bodrug, G. Young, R. T. VanderLinden, B. A. Schulman, J. Schimpf, T. Friedrich, P. V. Dip, T. U. Schwartz, B. Bauer, J. M. Peters, W. B. Struwe, J. L. P. Benesch, N. G. Brown, D. Haselbach, P. Kukura, Quantifying the heterogeneity of macromolecular machines by mass photometry. *Nat. Commun.* **11**, 1772 (2020).
49. J. Wang, J. Chen, Z. Gong, TopBP1 controls BLM protein level to maintain genome stability. *Mol. Cell* **52**, 667–678 (2013).
50. P. Picotti, R. Aebersold, Selected reaction monitoring-based proteomics: Workflows, potential, pitfalls and future directions. *Nat. Methods* **9**, 555–566 (2012).
51. L. Sun, L. Sun, Y. Huang, R. A. Edwards, S. Yang, A. N. Blackford, W. Niedzwiedz, J. N. M. Glover, Structural insight into BLM recognition by TopBP1. *Structure* **25**, 1582–1588.e3 (2017).
52. O. Addis Jones, A. Tiwari, T. Olukoga, A. Herbert, K. L. Chan, PLK1 facilitates chromosome biorientation by suppressing centromere disintegration driven by BLM-mediated unwinding and spindle pulling. *Nat. Commun.* **10**, 2861 (2019).
53. R. Bythell-Douglas, A. J. Deans, A structural guide to the bloom syndrome complex. *Structure* **29**, 99–113 (2021).
54. C. Frattini, A. Promonet, E. Alghoul, S. Vidal-Eychenie, M. Lamarque, M.-P. Blanchard, S. Urbach, J. Basbous, A. Constantinou, TopBP1 assembles nuclear condensates to switch on ATR signaling. *Mol. Cell* **81**, 1231–1245.e8 (2021).
55. A. Kim, K. Montales, K. Ruis, H. Senebandith, H. Gasparyan, Q. Cowan, W. M. Michael, Biochemical analysis of TOPBP1 oligomerization. *DNA Repair (Amst)* **96**, 102973 (2020).
56. K. L. Chan, P. S. North, I. D. Hickson, BLM is required for faithful chromosome segregation and its localization defines a class of ultrafine anaphase bridges. *EMBO J.* **26**, 3397–3409 (2007).
57. R. K. Clyne, V. L. Katis, L. Jessop, K. R. Benjamin, I. Herskowitz, M. Lichten, K. Nasmyth, Polo-like kinase Cdc5 promotes chiasmata formation and cosegregation of sister centromeres at meiosis I. *Nat. Cell Biol.* **5**, 480–485 (2003).
58. J. Matos, M. G. Blanco, S. C. West, Cell-cycle kinases coordinate the resolution of recombination intermediates with chromosome segregation. *Cell Rep.* **4**, 76–86 (2013).
59. T. J. Gaymes, P. S. North, N. Brady, I. D. Hickson, G. J. Mufti, F. V. Rassool, Increased error-prone non homologous DNA end-joining—A proposed mechanism of chromosomal instability in Bloom's syndrome. *Oncogene* **21**, 2525–2533 (2002).
60. I. Poser, M. Sarov, J. R. A. Hutchins, J. K. Hériché, Y. Toyoda, A. Pozniakovsky, D. Weigl, A. Nitzsche, B. Hegemann, A. W. Bird, L. Pelletier, R. Kittler, S. Hua, R. Naumann, M. Augsburg, M. M. Sykora, H. Hofemeister, Y. Zhang, K. Nasmyth, K. P. White, S. Dietzel, K. Mechtler, R. Durbin, A. F. Stewart, J. M. Peters, F. Buchholz, A. A. Hyman, BAC TransgeneOmics: A high-throughput method for exploration of protein function in mammals. *Nat. Methods* **5**, 409–415 (2008).
61. M. Petronczki, M. Glotzer, N. Kraut, J. M. Peters, Polo-like kinase 1 triggers the initiation of cytokinesis in human cells by promoting recruitment of the RhoGEF Ect2 to the central spindle. *Dev. Cell* **12**, 713–725 (2007).
62. D. M. Stults, M. W. Killen, A. J. Pierce, The sister chromatid exchange (SCE) assay. *Methods Mol. Biol.* **1105**, 439–455 (2014).
63. J. Matos, S. C. West, Analysis of structure-selective endonuclease activities from yeast and human extracts. *Methods Enzymol.* **591**, 271–286 (2017).
64. M. Gatti, R. Imhof, Q. Huang, M. Baudis, M. Altmeyer, The ubiquitin ligase TRIP12 limits PARP1 trapping and constrains PARP inhibitor efficiency. *Cell Rep.* **32**, 107985 (2020).
65. C. Pinto, K. Kasaciunaite, R. Seidel, P. Cejka, Human DNA2 possesses a cryptic DNA unwinding activity that functionally integrates with BLM or WRN helicases. *eLife* **5**, e18574 (2016).
66. L. N. Princz, P. Wild, J. Bittmann, F. J. Aguado, M. G. Blanco, J. Matos, B. Pfander, Dbf4-dependent kinase and the Rtt107 scaffold promote Mus81-Mms4 resolvase activation during mitosis. *EMBO J.* **36**, 664–678 (2017).
67. H. Goulaouic, T. Roulon, O. Flamand, L. Grondard, F. Lavelle, J. F. Riou, Purification and characterization of human DNA topoisomerase IIIalpha. *Nucleic Acids Res.* **27**, 2443–2450 (1999).
68. S. M. Howard, I. Ceppi, R. Anand, R. Geiger, P. Cejka, The internal region of CtIP negatively regulates DNA end resection. *Nucleic Acids Res.* **48**, 5485–5498 (2020).
69. R. Anand, C. Pinto, P. Cejka, Methods to study DNA end resection I: Recombinant protein purification. *Methods Enzymol.* **600**, 25–66 (2018).
70. E. W. Deutsch, H. Lam, R. Aebersold, PeptideAtlas: A resource for target selection for emerging targeted proteomics workflows. *EMBO Rep.* **9**, 429–434 (2008).
71. J. Cox, N. Neuhauser, A. Michalski, R. A. Scheltema, J. V. Olsen, M. Mann, Andromeda: A peptide search engine integrated into the MaxQuant environment. *J. Proteome Res.* **10**, 1794–1805 (2011).
72. K. Sarlós, A. S. Biebricher, A. H. Bizard, J. A. M. Bakx, A. G. Ferreté-Bonastre, M. Modesti, M. Paramasivam, Q. Yao, E. J. G. Peterman, G. J. L. Wuite, I. D. Hickson, Reconstitution of anaphase DNA bridge recognition and disjunction. *Nat. Struct. Mol. Biol.* **25**, 868–876 (2018).
73. C. Pinto, R. Anand, P. Cejka, Methods to study DNA end resection II: Biochemical reconstitution assays. *Methods Enzymol.* **600**, 67–106 (2018).
74. P. Cejka, J. L. Plank, C. Z. Bachrati, I. D. Hickson, S. C. Kowalczykowski, Rmi1 stimulates decatenation of double Holliday junctions during dissolution by Sgs1-Top3. *Nat. Struct. Mol. Biol.* **17**, 1377–1382 (2010).
75. K. Gari, C. Decaillet, A. Z. Stasiak, A. Stasiak, A. Constantinou, The Fanconi anemia protein FANCM can promote branch migration of Holliday junctions and replication forks. *Mol. Cell* **29**, 141–148 (2008).
76. I. Ceppi, S. M. Howard, K. Kasaciunaite, C. Pinto, R. Anand, R. Seidel, P. Cejka, CtIP promotes the motor activity of DNA2 to accelerate long-range DNA end resection. *Proc. Natl. Acad. Sci. U.S.A.* **117**, 8859–8869 (2020).

Acknowledgments: We thank B. Pfander for TOPBP1 and CDK2 expression constructs and members of the Cejka and Matos laboratories for critical reading of the manuscript. **Funding:** The Seidel laboratory is supported by a consolidator grant of the European Research Council (724863). The Altmeyer laboratory is supported by the Swiss National

Science Foundation (310030_197003), European Research Council (714326), and Swiss Cancer Research Foundation (KFS-4406-02-2018). The Cejka laboratory is supported by the Swiss National Science Foundation (31003A_175444) and European Research Council (681-630). The Matos laboratory was supported by ETH Zürich and is currently supported by the Swiss National Science Foundation (155823 and 176108), the Max Perutz Labs, and the University of Vienna. **Author contributions:** C.B.P. and S.G. performed all cellular work, with the exception of Fig. 4B and figs. S1, S2 (E and F), and S4A, which were contributed by V.P., and Fig. 4C and fig. S4 (E and F), which were contributed by N.P. M.G. and M.A. conducted QIBC experiments and analyzed results in fig. S2D. I.C. carried out all in vitro experiments with recombinant BLM, with the exception of mass photometry, which was carried out by K.K. and R.S. F.U. performed MS analyses. R.F. generated the anti-BLM antibody used for BLM IPs. J.M. and P.C. conceived the study and wrote the manuscript. All authors proofread and contributed to the final manuscript. **Competing interests:** The authors declare that they have no competing interests. **Data and materials availability:** All data needed to evaluate the conclusions in the paper are present in the paper and/or the Supplementary Materials. MS data have been deposited on PRIDE under identifiers PXD026460 and PXD026452.

Submitted 17 June 2021
Accepted 14 December 2021
Published 4 February 2022
10.1126/sciadv.abk0221